Lyapunov and minimum-time path planning for drones

Ugo Boscain*† Jean-Paul Gauthier‡† Thibault Maillot‡ Ulysse Serres§

July 8, 2013

Abstract

In this paper, we study the problem of controlling an unmanned aerial vehicle (UAV) to provide a target supervision and/or to provide convoy protection to ground vehicles.

We first present a control strategy based upon a Lyapunov-LaSalle stabilization method to provide supervision of a stationary target . The UAV is expected to join a fixed target (a point in the space) and turn around tracking a pre-designed admissible circular trajectory.

Our strategy is presented for both HALE (High Altitude Long Endurance) and MALE (Medium Altitude Long Endurance) types UAVs. A UAV flying at a constant altitude (HALE type) is modeled as a Dubins vehicle (i.e. a planar vehicle with constrained turning radius and constant forward velocity). For a UAV that might change its altitude (MALE type), we use the general kinematic model of a rigid body evolving in $\mathbb{R}^3$. Both control strategies presented are smooth and unlike what is usually proposed in the literature these strategies asymptotically track a circular trajectory of exact minimum turning radius.

We also present the time-optimal control synthesis for tracking a circle by a Dubins vehicle. This optimal strategy, although much simpler than the point-to-point time-optimal strategy obtained by P. Souères and J.-P. Laumond in the 1990s (see [43]), is very rich.

Finally, we propose control strategies to provide supervision of a moving target , that are based upon the previous ones.

Keywords: optimal control, path planning, aircraft navigation, surveillance, unmanned aerial vehicles, rigid-body dynamics, under-actuated systems, nonlinear control, thrust-propelled vehicle, trajectory tracking.

1 Introduction

This study holds in the context of the French FUI SHARE project (see [3]), supported by a consortium of companies and research labs [1], and the authors are granted from the project. The aim is to design a trajectory for a UAV from some starting point and orientation to some final submanifold of the state space.

The UAV path planning problem is a standard motion planning problem and although the bibliography on this subject is very rich we do not aim to provide an exhaustive list. Let us just mention that classical planning algorithms are based upon very different approaches such as geometric control [14, 18, 31], optimal control [20], flatness [7], stochastic theory [5].

*Centre de Mathématiques Appliquées - Ecole Polytechnique (CMAP), UMR CNRS 7641, Route de Saclay, 91128 Palaiseau Cedex, France; email: ugo.boscain@polytechnique.edu

†INRIA GECO Project

‡Université du Sud-Toulon-Var, LSIS, UMR CNRS 7296, B.P 20132, 83957 La Garde Cedex, France; email: jean-paul.gauthier@univ-tln.fr & thibault.maillot@univ-tln.fr

§Université de Lyon, F-69 622 Lyon, France; Université Lyon 1, Villeurbanne; LAGEP, UMR CNRS 5007, 43 bd du 11 novembre 1918, 69100 Villeurbanne, France; email: ulysse.serres@univ-lyon1.fr

[1] Opéra Ergonomie, ONERA, Thales Alénia Space, Eurocopter, Adetel group.

Moreover, the reader may refer to [26] for a survey on trajectory-planning algorithms focusing on autonomous UAV guidance.

The purpose of this paper is to present different solutions to the above mentioned planification problem for both HALE and MALE types of fixed-wing UAVs. Although the case of rotary-wing drones is interesting, it is simpler and more standard motion planning methods may be applied (see [8, 25]).

The problem is addressed from a kinematic point of view only. In particular, we consider that the aircraft controls are just the angular velocities. From a kinematic point of view, a UAV can be specified by a control system $\dot{q} = f(q, u)$ (specific models will be given later on), where q denotes the state of the UAV which usually includes the UAV position (in $\mathbb{R}^2$ or $\mathbb{R}^3$) and attitude (i.e. the UAV orientation in S^1 or $SO(3)$), and u is the control vector driving the UAV kinematics, such as angular and spacial velocities. Moreover, we make the following assumptions on the UAV:

- the velocity of the UAV is assumed to have a positive lower bound (no stationary or quasistationary flights are allowed) and a positive upper bound;
- the UAV is assumed to be kinematically restricted by its minimum turning radius $r > 0$, or equivalently, its yaw angle is assumed to be constrained by an upper positive bound.

In this article, tools from Lyapunov-based stability analysis and optimal control theory are used for the development of control algorithms achieving the desired motion planning task.

The paper is organized as follows: in Section 2, we present global Lyapunov-LaSalle-based stabilization results for a UAV tracking a horizontal circle of minimal turning radius. Section 2.1 and Section 2.2 are the detailed studies of the cases of HALE and MALE UAVs respectively.

Section 3 describes the time-optimal synthesis for the Dubins system tracking a minimal radius circle. The study is done in a reduced state space. On this subject, we have to mention the great work [43] about the more complicated point-to-point problem (see also [1] for a partial study).

Finally, in Section 4 the results of Sections 2 and 2.2 are brought together and an algorithm for the tracking of a moving target is proposed. In the present paper, what is meant by *target* is the position (in $\mathbb{R}^2$ or $\mathbb{R}^3$) of the center of mass of the object the UAV has to follow.

We end this introductory section providing a list of mathematical conventions used here in. In the paper, smooth means C^∞. Throughout the remaining of the paper, the time dependence of variables is often omitted to lighten notations. Moreover, we use

- the dot $\dot{}$ to denote the derivative with respect to time;
- $|x|$ to denote the usual Euclidean norm of $x \in \mathbb{R}^n$, and $\langle x, y \rangle$ for the inner product of two such vectors;
- $B(x, r) \subset \mathbb{R}^n$ to denote the open ball of radius r centered at x;
- M' to denote the transpose of a matrix M;
- $\mathrm{tr}(M) = \sum_{i=1}^n M_{ii}$ to denote the trace of a $n \times n$ square matrix M;
- $[\cdot, \cdot]$ to denote the Lie bracket between vector fields and the commutator of matrices.

- For two $n \times n$ real matrices M and N, the Hilbert-Schmidt scalar product is $\mathrm{tr}(M'N)$, then the Hilbert-Schmidt norm of a matrix M is $\sqrt{\mathrm{tr}(M'M)}$.
- Also, we do not distinguish between row and column vectors, the distinction being clear from the context.

2 Lyapunov-LaSalle-based stabilization

This section is concerned with the problem of global stabilization of a UAV (in the position-attitude state space) on a fixed horizontal circle of minimum turning radius with prescribed direction that we shall refer to as the "final manifold".

By using a standard Lyapunov-LaSalle-based approach, we propose, for both HALE and MALE type UAVs, new nonlinear feedback control laws that stabilize the UAV on the final manifold.

The Lyapunov method has been used by several authors, in different ways such as for example [15, 16, 19, 21, 23, 27, 32, 34, 48]. Here we present an original Lyapunov strategy, serving the advantage to be completely smooth, very simple to apply, and with the peculiarity that the circular final manifold is with exactly minimum turning radius. Frequently, Lyapunov strategies presented in the literature do not have this last feature.

2.1 Lyapunov based method for the Dubins system

2.1.1 Problem under consideration

From the kinematic point of view, a rough HALE drone is governed by the standard Dubins equations (see e.g. [17] for a justification):

$$\begin{cases} \dot{x} = \cos\theta \\ \dot{y} = \sin\theta \\ \dot{\theta} = u. \end{cases} \tag{2.1}$$

with $(x, y, \theta) \in \mathbb{R}^2 \times \mathbb{S}^1$ being the state (where $(x, y) \in \mathbb{R}^2$ is the UAV's coordinate in the constant altitude plane, and θ the yaw angle), and $u \in [-u_{\max}, u_{\max}]$ being the control variable. Note that the yaw angle θ is the angle made by the aircraft direction with respect to the x-axis.

These equations express that the drone evolves on a perfect plane (perfect constant altitude), at perfect constant speed 1, moves in the direction of its velocity vector, and is able to turn right and left.

Note that the rough model (2.1) is pertinent for HALE drones, the velocity being almost really constant.

As said in the introduction, the UAV is assumed to be kinematically restricted by its positive minimum turning radius r which implies the following bound on the yaw anglular velocity:

$$-\frac{1}{r} = -u_{\max} \leqslant u \leqslant u_{\max} = \frac{1}{r}.$$

Remark 2.1. Note that up to a dilation in the (x, y)-plane we may assume without loss of generality that $[-u_{\max}, u_{\max}] = [-1, 1]$.

We denote by $\mathcal{C}$ the final manifold which is defined to be the counterclockwise oriented circle centered at the origin of the (x, y)-plane, with radius $r = 1/u_{\max}$. In the (x, y, θ)-coordinates system, $\mathcal{C}$ is given by

$$\mathcal{C} = \{(x, y, \theta) \mid x = r \sin\theta,\ y = -r\cos\theta\}.$$

We have the following result.

Theorem 2.2. *There exists a smooth feedback control $k : \mathbb{R}^2 \times \mathbb{S}^1 \to [-u_{\max}, u_{\max}]$ such that the set $\mathcal{C}$ is a globally asymptotically stable attractor for the closed-loop system resulting from applying the feedback control $u = k(x, y, \theta)$ to system (2.1).*

2.1.2 Proof of theorem 2.2

The proof of Theorem 2.2 is based upon a standard Lyapunov-based control design and LaSalle's principle (see e.g. [24, Theorem 3.5, p.190] or the original LaSalle's paper [30]).

To construct a state feedback stabilizer to $\mathcal{C}$ for system (2.1) (and further to construct the time-optimal synthesis in Section 3), it is convenient to use UAV-based coordinates $(\tilde{x}, \tilde{y}, \theta)$ with $\tilde{x}$ and $\tilde{y}$ defined by

$$\begin{pmatrix} \tilde{x} \\ \tilde{y} \end{pmatrix} = \begin{pmatrix} \cos\theta & \sin\theta \\ -\sin\theta & \cos\theta \end{pmatrix} \begin{pmatrix} x \\ y \end{pmatrix},$$

in which the set $\mathcal{C} = \{(\tilde{x}, \tilde{y}, \theta) \mid \tilde{x} = 0,\ \tilde{y} = -r\}$. Notice that if $\mathcal{C}$ would have been travelled clockwise, the equation $\tilde{y} = -r$ would have been changed for $\tilde{y} = r$.

In the $(\tilde{x}, \tilde{y})$-coordinates system, the two first equations of system (2.1) may be rewritten as

$$\begin{cases} \dot{\tilde{x}} = u\tilde{y} + 1 \\ \dot{\tilde{y}} = -u\tilde{x}. \end{cases} \tag{2.2}$$

Remark 2.3. One can read, in (2.2) that if u is changed for $-u$, the two equilibria of (2.2) corresponding to the control values $-u_{\max}$ and $u_{\max}$ are exchanged so that the set of equilibria remains unchanged. It means that we can indifferently consider one of the two equilibria positions.

Changing the $(\tilde{x}, \tilde{y})$ coordinates for $(\bar{x}, \bar{y}) = (\tilde{x}, \tilde{y} + r)$, the stabilization problem to $\mathcal{C}$ is reformulated in these variables as the stabilization problem to the submanifold $\{(\bar{x}, \bar{y}, \theta) \mid \bar{x} = \bar{y} = 0\}$. Equivalently, we will refer to the convergence of $(\bar{x}, \bar{y})$ to the point $(0, 0)$ of the *reduced state space*. The reader can easily check that the $(\bar{x}, \bar{y})$ obey the following equations:

$$\begin{cases} \dot{\bar{x}} = u\bar{y} + 1 - ru \\ \dot{\bar{y}} = -u\bar{x}. \end{cases} \tag{2.3}$$

The proof of Theorem 2.2 is a consequence of its analogue in the reduced $(\bar{x}, \bar{y})$-coordinate state space.

Lemma 2.4. *There exists a (smooth) feedback control $k : \mathbb{R}^2 \to [-u_{\max}, u_{\max}]$ which stabilizes trajectories of the system (2.3) with $u(t) = \bar{k}(\bar{x}(t), \bar{y}(t))$ with respect to the origin.*

Proof. We shall prove that

$$V(\bar{x}, \bar{y}) = \bar{x}^2 + \bar{y}^2$$

is a Lyapunov function for system (2.3) if the control law is well chosen. A straightforward computation yields

$$\dot{V}(\bar{x}, \bar{y}) = 2\bar{x}\,(1 - ru).$$

To be a Lyapunov function for system (2.3), we need to ensure that $\dot{V}$ is nonpositive. Keeping in mind that $u_{\max} = 1/r$, it yields $u = u_{\max}$ when $\bar{x} \geqslant 0$. Let ε be a positive real number, let a be such that $-u_{\max} \leqslant a < u_{\max}$ and let $k : \mathbb{R}^2 \to [-u_{\max}, u_{\max}]$ be a (actually any) smooth feedback control which satisfies

$$\bar{k}(\bar{x}, \bar{y}) = \begin{cases} u_{\max} & \text{if } \bar{x} \geqslant 0 \\ u_{\max} > \bar{k}(\bar{x}, \bar{y}) \geqslant -u_{\max} & \text{if } \bar{x} < 0. \end{cases} \tag{2.4}$$

For instance, one can take the function defined by

$$\bar{k}(\bar{x}, \bar{y}) = \begin{cases} a & \text{if } \bar{x} \leqslant -\varepsilon \\ \frac{u_{\max} - a}{1 + e^{1/(\bar{x}+\varepsilon)+1/\bar{x}}} + a & \text{if } \bar{x} \in (-\varepsilon, 0) \\ u_{\max} & \text{if } \bar{x} \geqslant 0, \end{cases}$$

the shape of which is drawn on the next figure.

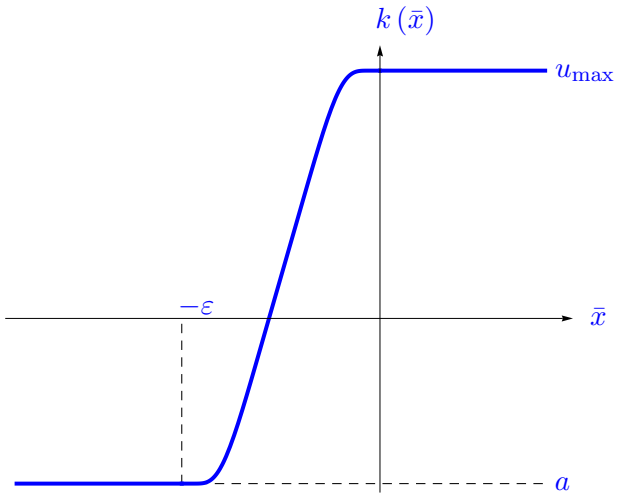

According to LaSalle's principle and since V is a proper function, we infer that all the trajectories of system (2.3) with feedback control $\bar{k}(\cdot)$ converge to the largest invariant set contained in the set $E = \{(\bar{x}, \bar{y}) \mid \dot{V}(\bar{x}, \bar{y}) = 0\} = \{(\bar{x}, \bar{y}) \mid \bar{x} \geqslant 0\}$. Due to condition (2.4) on the feedback control, it is easy to see that any solution to (2.3) starting at $(\bar{x}_0, \bar{y}_0)$ with $\bar{x}_0 > 0$ escapes from E in finite time. Indeed, when $x_0 > 0$ the solution to the closed-loop system satisfies on E:

$$\begin{cases} \dot{\bar{x}} = u_{\max} \bar{y} \\ \dot{\bar{y}} = -u_{\max} \bar{x}. \end{cases}$$

A REFAIRE

Hence, the solution $(\bar{x}(t), \bar{y}(t)) = (\bar{x}_0 \cos(u_{\max} t) - \bar{y}_0 \sin(u_{\max} t), \bar{x}_0 \sin(u_{\max} t) + \bar{y}_0 \cos(u_{\max} t))$ **escapes from** E **at time**

$$t = \begin{cases} \frac{1}{u_{\max}} \left(\pi + \arctan\left(\frac{\bar{x}_0}{\bar{y}_0} \right) \right) & \textbf{if } \bar{y}_0 < 0 \\ \frac{\pi}{2u_{\max}} & \textbf{if } \bar{y}_0 = 0 \\ \frac{1}{u_{\max}} \arctan\left(\frac{\bar{x}_0}{\bar{y}_0} \right) & \textbf{if } \bar{y}_0 > 0. \end{cases}$$

Consequently, the largest invariant set contained in E is the equilibrium point $(0, 0)$. This ends the proof. ■

Proof of Theorem 2.2. Since $V(\bar{x}, \bar{y})$ tends to zero implies that (x, y, θ) tends to $\mathcal{C}$, Lemma (2.4) shows that $\bar{k}$ steers asymptotically system (2.3) to $\mathcal{C}$, or equivalently that $k(x, y, \theta) = \bar{k}(\phi(x, y, \theta))$, (where $\phi : (x, y, \theta) \mapsto (\bar{x}, \bar{y})$) steers asymptotically system (2.1) to $\mathcal{C}$. ■

2.1.3 Numerical results

The theory exposed in the preceding subsections was tested by means of simulated data. During these simulations, we numerically integrate the closed-loop system resulting from applying the feedback control $u = k(x, y, \theta)$ of Theorem 2.2 to system (2.1) during 200 units of time.

Figure 1 shows two trajectories of the same UAV starting from the same initial point but with two different values of the parameter ε in the control function defined by equation (2.4). On both pictures the UAV reaches the final manifold tangentially, here the circle of radius 2 centered at the origin.

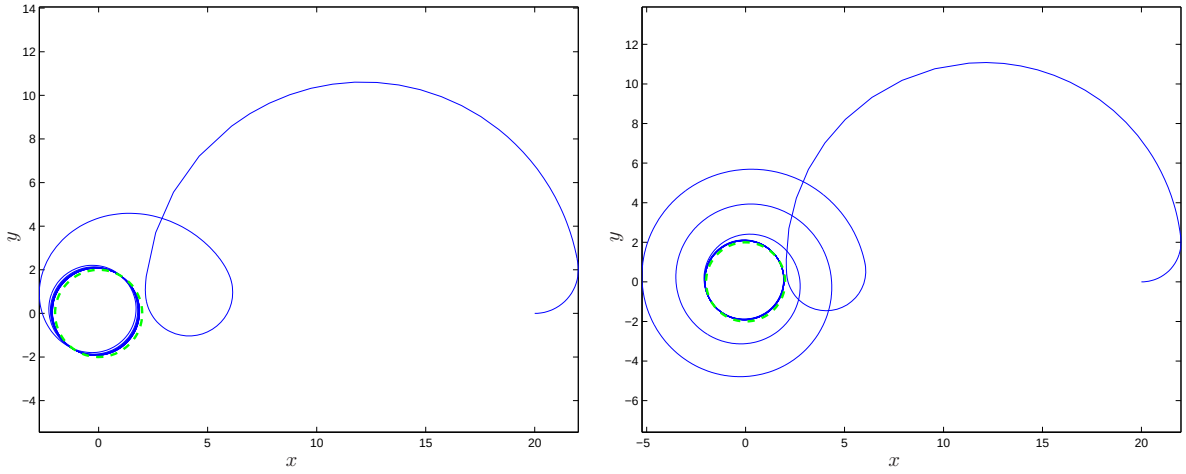

(a) (b)

Figure 1: Illustration of Lyapunov-LaSalle's-based 2D-planification results with starting point $(x_0, y_0, \theta_0) = (20, 0, 0)$, control constraints $u_{\max} = 0.5$ and $a = 0.1$. (a) $\varepsilon = 2$, (b) $\varepsilon = 0.5$.

2.2 Extension of the method to the 3D case

2.2.1 Statement of the problem and of the result

In this section, we extend the results of the previous section to the case of MALE UAVs flying at constant speed. Our goal is unchanged: we want to (globally) stabilize the UAV on a final manifold .

From the kinematic point of view, a rough MALE drone (modeled by a standard 6 degree of freedom solid, symmetric w.r.t. its vertical middle plane) is governed by the following equations

$$\begin{cases} \dot{X} = RV_0 \\ \dot{R} = R\Omega \end{cases} \tag{2.5}$$

with

- $Q = (X, R) \in \mathbb{R}^3 \times SO(3)$ being the state where X is the UAV's coordinates expressed in the inertial frame and R, the UAV attitude, is the rotation matrix between the UAV's fixed frame and the inertial frame which gives the motion of the UAV's frame orientation;
- $V_0 = (1, 0, 0)$ being the thrust direction expressed in the UAV's frame;

- and $\Omega = \begin{pmatrix} 0 & -u_3 & u_2 \\ u_3 & 0 & -u_1 \\ -u_2 & u_1 & 0 \end{pmatrix} \in \mathfrak{so}(3)$ (the Lie algebra of $SO(3)$ consisting of skew-symmetric matrices) the angular velocity of the body expressed in the body-fixed frame.

System (2.5) is used by many authors in the litterature to model UAVs and airplanes (see e.g. [28, 46]). See also [47] and references therein. We define $u = (u_1, u_2, u_3)$ to be the control variables and we denote by $U = \prod_{i=1}^{3}[-u_{i\max}, u_{i\max}]$ the control set. The control variables are the roll (u_1), pitch (u_2) and yaw (u_3) angular velocities and are constrained by $u_{i\max} > 0$ for $i = 1, 2, 3$.

Remark 2.5. Notice that the controlability of system (2.5) with control in U is a direct consequence of [9, Theorem 1] (see also [39, Theorem 6.7]).

Equations (2.5) express that the drone moves in a 3-dimensional space, at perfect constant speed 1, moves in the direction of its velocity vector, and is able to turn in every direction of its fixed frame.

The First equation of system (2.5), in $\mathbb{R}^3$, describes the evolution of the UAV in space. The second one, in $SO(3)$, depicts the motion of the UAV's frame which is controlled by three controls on angular velocity acting physically on the roll, pitch and yaw angles.

Set $X = (x_1, x_2, x_3)$. The (x_1, x_2)-plane is called the horizontal plane. Here, we fix the final manifold $\mathcal{C}$ to be the union $\mathcal{C} = \mathcal{C}_1 \cup \mathcal{C}_2$ of the two circles of radius $r_3 = 1/u_{3\max}$ centered at the origin in the horizontal (x_1, x_2)-plane and oriented counterclockwise in the orientation given by their normals $N_1 = (0, 0, 1)$, $N_2 = (0, 0, -1)$. Define

$$J_1 = \begin{pmatrix} 0 & 0 & 0 \\ 0 & 0 & -1 \\ 0 & 1 & 0 \end{pmatrix}, \quad J_2 = \begin{pmatrix} 0 & 0 & 1 \\ 0 & 0 & 0 \\ -1 & 0 & 0 \end{pmatrix}, \quad J_3 = \begin{pmatrix} 0 & -1 & 0 \\ 1 & 0 & 0 \\ 0 & 0 & 0 \end{pmatrix},$$

so that $\Omega = u_1 J_1 + u_2 J_2 + u_3 J_3$.

Notice that the Lie algebra structure on $\mathfrak{so}(3)$ is given by

$$[J_1, J_2] = J_3, \quad [J_2, J_3] = J_1, \quad [J_3, J_1] = J_2. \tag{2.6}$$

The reader can easily check that, in the (X, R)-coordinates system, the final manifold takes the form: $\mathcal{C} = \mathcal{C}_1 \cup \mathcal{C}_2$, setting $\Delta_1 = \begin{pmatrix} 1 & 0 & 0 \\ 0 & -1 & 0 \\ 0 & 0 & -1 \end{pmatrix}$,

$$\mathcal{C}_1 = \left\{(X, R) \in \mathbb{R}^3 \times SO(3) \mid X = r_3(\sin\theta, -\cos\theta, 0),\ R = e^{J_3\theta},\ \theta \in \mathbb{R}\right\}$$

$$\mathcal{C}_2 = \left\{(X, R) \in \mathbb{R}^3 \times SO(3) \mid X = r_3(\sin\theta, \cos\theta, 0),\ R = \Delta_1 e^{J_3\theta},\ \theta \in \mathbb{R}\right\}.$$

We will prove the following result.

Theorem 2.6. *There exists a (smooth) feedback control $k : \mathbb{R}^3 \times SO(3) \to U$ such that the set $\mathcal{C}$ is a global asymptotic attractor for the closed-loop system resulting from applying the feedback control $u = k(X, R)$ to system (2.5). Moreover $\mathcal{C}_1$ is an asymptotically stable limit cycle and $\mathcal{C}_2$ is an unstable limit cycle. All trajectories tend to $\mathcal{C}_1$ but the trajectories starting in the plane $x_3 = 0$ with $R(0) = \Delta_1 e^{J_3\theta}$ for some θ, which tend to $\mathcal{C}_2$.*

2.2.2 Proof of Theorem 2.6

Here again, to construct a state feedback stabilizer to $\mathcal{C}$ for system (2.5) it is convenient to use UAV-based coordinates $(\tilde{X}, R)$ defined by $X = R\tilde{X}$ in which $\tilde{X}$ obeys

$$\dot{\tilde{X}} = V_0 - \Omega\tilde{X},$$

and the final manifold takes the form $\tilde{\mathcal{C}} = \tilde{\mathcal{C}}_1 \cup \tilde{\mathcal{C}}_2$,

$$\tilde{\mathcal{C}}_1 = \left\{ \left(\tilde{X}, R\right) \in \mathbb{R}^3 \times SO(3) \;\middle|\; \tilde{X} = (0, -r_3, 0),\ R = e^{J_3\theta},\ \theta \in \mathbb{R} \right\},$$

$$\tilde{\mathcal{C}}_2 = \left\{ \left(\tilde{X}, R\right) \in \mathbb{R}^3 \times SO(3) \;\middle|\; \tilde{X} = (0, -r_3, 0),\ R = \Delta_1 e^{J_3\theta},\ \theta \in \mathbb{R} \right\}.$$

Set $\tilde{X}^* = (0, -r_3, 0)$ and consider the new variable

$$\bar{X} = \tilde{X} - \tilde{X}^*.$$

It yields the new system

$$\begin{cases} \dot{\bar{X}} = V_0 - \Omega\left(\bar{X} + \tilde{X}^*\right) \\ \dot{R} = R\Omega. \end{cases} \tag{2.7}$$

In particular, we have

$$\begin{cases} \dot{\bar{x}}_1 = u_3\bar{x}_2 - u_2\bar{x}_3 + (1 - r_3u_3) \\ \dot{\bar{x}}_2 = -u_3\bar{x}_1 + u_1\bar{x}_3 \\ \dot{\bar{x}}_3 = u_2\bar{x}_1 - u_1\bar{x}_2 + r_3u_1. \end{cases}$$

The stabilization problem to $\tilde{\mathcal{C}}$ is reformulated in these variables as the stabilization problem to the submanifold $\bar{\mathcal{C}} = \bar{\mathcal{C}}_1 \cup \bar{\mathcal{C}}_2$,

$$\bar{\mathcal{C}}_1 = \left\{ \left(\bar{X}, R\right) \in \mathbb{R}^3 \times SO(3) \;\middle|\; \bar{X} = 0, \quad R = e^{J_3\theta}, \quad \theta \in \mathbb{R} \right\}.$$

$$\bar{\mathcal{C}}_2 = \left\{ \left(\bar{X}, R\right) \in \mathbb{R}^3 \times SO(3) \;\middle|\; \bar{X} = 0, \quad R = \Delta_1 e^{J_3\theta}, \quad \theta \in \mathbb{R} \right\}.$$

Let σ be a positive real number. We shall prove that the function $V : \mathbb{R}^3 \times SO(3) \to \mathbb{R}_+$ defined by

$$\begin{aligned} V(\bar{X}, R) &= \frac{1}{2}\left(\sigma\bar{X}'\bar{X} + \operatorname{tr}\left([R, J_3]'[R, J_3]\right)\right) \\ &= V_1(\bar{X}, R) + V_2(\bar{X}, R) \text{ with,} \end{aligned} \tag{2.8}$$

$V_1(\bar{X}, R) = \frac{1}{2}\left(\sigma\bar{X}'\bar{X}\right)$ and $V_2(\bar{X}, R) = \frac{1}{2}\left(\operatorname{tr}\left([R, J_3]'[R, J_3]\right)\right)$

is a Lyapunov function for the closed-loop system resulting from applying a well-chosen feedback control $u = k(\bar{X}, R)$ to (2.7).

Remark 2.7. Notice that the coefficient σ in the Lyapunov function (2.8) is a weight parameter that can be tuned in order to give more (resp. less) importance to the horizontality (i.e., pitch and roll angles close to zero) of the drone rather than its distance (in $\mathbb{R}^3$) to the target if $\sigma < 1$ (resp. $\sigma > 1$) during the stabilization process. Although this parameter plays no role in the subsequent results and computations, we keep it in our formulas.

The function V is clearly smooth. Moreover, the following proposition is obvious.

Proposition 2.8. *$V(\cdot)$ is a proper function.*

Notice that $V\left(\bar{X},R\right)$ may be rewritten as

$$V(\bar{X},R)=\frac{\sigma}{2}\bar{X}'\bar{X}+2+\mathrm{tr}\left(RJ_3R'J_3\right).$$

Hence, taking into account equations (2.6), the derivation w.r.t. time of $V\left(\bar{X},R\right)$ along the trajectories of system (2.7) yields

$$\begin{aligned}\dot{V}\left(\bar{X},R\right) &= \sigma\bar{X}'\dot{\bar{X}}+\frac{d}{dt}\mathrm{tr}\left(RJ_3R'J_3\right)\\ &= \sigma\bar{X}'\big(V_0-\Omega\big(\bar{X}+\tilde{X}^*\big)\big)+\mathrm{tr}\left(R[\Omega,J_3]R'J_3\right)\\ &= \sigma\bar{X}'\big(V_0-\Omega\tilde{X}^*\big)+\mathrm{tr}\big(R(u_1[J_1,J_3]+u_2[J_2,J_3]R)J_3\big)\\ &= \sigma\left\langle\begin{pmatrix}\bar{x}_1\\ \bar{x}_2\\ \bar{x}_3\end{pmatrix},\begin{pmatrix}1\\0\\0\end{pmatrix}+(u_1J_1+u_3J_3)\begin{pmatrix}0\\r_3\\0\end{pmatrix}\right\rangle-u_1\mathrm{tr}\left(RJ_2R'J_3\right)+u_2\mathrm{tr}\left(RJ_1R'J_3\right)\\ &= \sigma\bar{x}_1\left(1-r_3u_3\right)+u_1\left(\sigma r_3\bar{x}_3-\mathrm{tr}\left(RJ_2R'J_3\right)\right)+u_2\mathrm{tr}\left(RJ_1R'J_3\right).\end{aligned}$$

Remark 2.9. Note that $\dot{V}_1\left(\bar{X},R\right)=\sigma\bar{x}_1\left(1-r_3u_3\right)$ and $\dot{V}_2\left(\bar{X},R\right)=u_1\left(\sigma r_3\bar{x}_3-\mathrm{tr}\left(RJ_2R'J_3\right)\right)+u_2\mathrm{tr}\left(RJ_1R'J_3\right)$. Later it will be important that both quantities will be negative.

Let ε be a (small) positive real number. Set $\xi_1=\sigma r_3\bar{x}_3-\mathrm{tr}\left(RJ_2R'J_3\right)$ and $\xi_2=\mathrm{tr}\left(RJ_1R'J_3\right)$. In order to ensure the non positiveness of $\dot{V}$, we choose smooth feedback controls $u_1=k_1(\bar{X},R)$, $u_2=k_2(\bar{X},R)$ and $u_3=k_3(\bar{X},R)$ such that:

$$\mathrm{sign}\,k_1(\bar{X},R)=-\,\mathrm{sign}\,\xi_1 \tag{2.9}$$

$$\mathrm{sign}\,k_2(\bar{X},R)=-\,\mathrm{sign}\,\xi_2 \tag{2.10}$$

$$k_3(\bar{X},R)=\begin{cases}u_{3\max} & \text{if } \bar{x}_1\geqslant 0\\ -u_{3\max}\leqslant k_3(\bar{X},R)<u_{3\max} & \text{if } \bar{x}_1<0.\end{cases} \tag{2.11}$$

The feedback controls k_1, k_2 may be rewritten as

$$\begin{aligned}k_1(\bar{X},R)&=-\xi_1\varphi_1\left(\xi_1\right),\\ k_2(\bar{X},R)&=-\xi_2\varphi_2\left(\xi_2\right),\end{aligned}$$

where φ_1, φ_2 are smooth strictly positive functions and ξ_1 (resp. ξ_2) is zero if and only if $u_1=0$ (resp. $u_2=0$). Hence,

$$\dot{V}\left(\bar{X},R\right)=\sigma\bar{x}_1\left(1-r_3u_3\right)-\xi_1^2\varphi_1\left(\xi_1\right)-\xi_2^2\varphi_2\left(\xi_1\right).$$

According to LaSalle's principle and since V is a proper function, we infer that all the trajectories of system (2.7) with feedback controls k_1, k_2 and k_3 converge to the largest invariant set I contained in the set

$$\begin{aligned}E&=\{(\bar{X},R)\mid\dot{V}(\bar{X},R)=0\}\\ &=\{(\bar{X},R)\mid k_1(\bar{X},R)=k_2(\bar{X},R)=0,\ k_3(\bar{X},R)=u_{3\max}\}\\ &=\{(\bar{X},R)\mid\xi_1=\xi_2=0,\ k_3(\bar{X},R)=u_{3\max}\}.\end{aligned} \tag{2.12}$$

Obviously we have $\bar{\mathcal{C}}\subset I$. Let us prove the converse. Due to conditions (2.12) on the feedback controls, it is easy to see that any solution to (2.5) starting from $(\bar{X},R)\in E$ and

remaining in E satisfies

$$\begin{cases} \dot{\bar{x}}_1 = u_{3\max}\bar{x}_2 \\ \dot{\bar{x}}_2 = -u_{3\max}\bar{x}_1 \\ \dot{\bar{x}}_3 = 0 \\ \dot{R} = Ru_{3\max}J_3. \end{cases} \tag{2.13}$$

Consequently, any solution to (2.13) starting from I with $\bar{x}_1 > 0$ escapes from E in finite time. Thus, any point in I satisfies $\bar{x}_1 = 0$ and consequently, due to the first equation of system (2.13), $\bar{x}_2 = 0$. Moreover, according to the third equation of system (2.13) $\bar{x}_3$ is constant in E. This constant is easily seen to be equal to zero. Indeed, let $t \mapsto \left(\bar{X}(t), R(t)\right)$ be a smooth curve in I defined on an interval around zero. Since the functions ξ_1 and ξ_2 are identically zero in E, we have

$$\sigma r_3 \bar{x}_3 = \mathrm{tr}\left(RJ_2R'J_3\right), \tag{2.14}$$

$$0 = \mathrm{tr}\left(RJ_1R'J_3\right). \tag{2.15}$$

Since $\bar{x}_3$ is constant, differentiation of equation (2.15) (divided by $u_{3\max}$) w.r.t. t yields

$$\begin{aligned} 0 &= \frac{1}{u_{3\max}}\frac{d}{dt}\mathrm{tr}\left(RJ_1R'J_3\right) \\ &= \frac{1}{u_{3\max}}\mathrm{tr}\left(R[u_{3\max}J_3, J_1]R'J_3\right) \\ &= \mathrm{tr}\left(RJ_2R'J_3\right), \end{aligned} \tag{2.16}$$

which, according to (2.14), implies that $\bar{x}_3 = 0$. Summing up, we get $I \subset \{\bar{x}_1 = \bar{x}_2 = \bar{x}_3 = 0\}$. It remains to show that R has the required form. Equations 2.15 and 2.16 may be rewritten as $\mathrm{tr}\left(J_1(R'J_3R)\right) = 0$ and $\mathrm{tr}\left(J_2(R'J_3R)\right) = 0$ showing that $R'J_3R$ is orthogonal to J_1 and J_2 for the Hilbert-Schmidt scalar product. It follows that $R'J_3R = \lambda J_3$ with $\lambda \in \mathbb{R}$. Moreover, conjugations by elements of $SO(3)$ being isometries for the Hilbert-Schmidt scalar product, we must have $|\lambda| = 1$. Consequently, $R'J_3R = \pm J_3$. The case $\lambda = +1$ exactly means that the rotation matrix R commutes with J_3. According to Lemma 2.10 below, R is of the form $e^{J_3\theta}$. The case $\lambda = -1$ is similar and we conclude that R is of the form $\Delta_1 e^{J_3\theta}$.

It is clear that all trajectories $\mathcal{T}(t)$ starting in the plane $\{\bar{x}_3 = 0\}$ with $R(0) = \Delta_1 e^{J_3\theta}$ tend to $\bar{\mathcal{C}}_2$ since $u_1 \equiv 0$, $u_2 \equiv 0$.

Let us show that any other trajectory tends to $\bar{\mathcal{C}}_1$. Due to Remark 2.9, $\dot{V}_2 \leqslant 0$ then V_2 cannot increase along any trajectory. But V_2 reaches its maximum exactly on the union of the trajectories of type $\mathcal{T}(t)$.

Lemma 2.10. *The stabilizer $\mathcal{S}_3$ of J_3 under conjugation by $SO(3)$ is the subgroup of rotations R_3 about the x_3-axis, $R_3 = \begin{pmatrix} \cos\theta & \sin\theta & 0 \\ -\sin\theta & \cos\theta & 0 \\ 0 & 0 & 1 \end{pmatrix}$.*

Proof. With obvious block notations, write $J_3 = \begin{pmatrix} J & 0 \\ 0 & 0 \end{pmatrix}$ and $H = \begin{pmatrix} A & B \\ C & d \end{pmatrix}$. Then, $[J_3, H] = \begin{pmatrix} [J,A] & JB \\ -CJ & 0 \end{pmatrix}$. For $H \in \mathcal{S}_3$, $H'J_3H = J_3$, which is equivalent to $[J_3, H] = 0$. It implies that $B = 0$, $C = 0$ and $[J, A] = 0$. Since $H \in SO(3)$, we first conclude that $d = \pm 1$ and $A \in O(2)$.

The stabilizer of J under conjugation by $O(2)$ is $SO(2)$. Then, $A \in SO(2)$, $\det(A) = 1$, and $d = 1$. Therefore, H is of the form R_3. ∎

2.2.3 Numerical results

The theory exposed in the preceding subsections was tested by means of simulated data. During these simulations, we numerically integrate the closed-loop system resulting from applying the feedback control $u = (u_1, u_2, u_3) = (k_1(X, R), k_2(X, R), k_3(X, R))$ of Theorem 2.6 to system (2.5) during 200 units of time.

The feedback control k_3 is built as its analogue k in the 2D-case. Concerning the feedback controls k_1 and k_2 we chose smooth functions varying slowly between the minimum and the maximum control constraints.

Figures 2 and 3 display trajectories obtained for the same UAV which starts at the point $(50, 20, 20)$ with a direction of 0 radian for the pitch, roll and yaw angles. We consider the following curvature constraints, $u_{1\max} = u_{2\max} = -u_{1\min} = -u_{2\min} = 0.1$, $u_{3\max} = 0.5$, $u_{3\min} = 0.1$.

The difference between Figure 2 and Figure 3 is due to the value of the parameter ε in the control function defined in equation (2.11). In the first case we set $\varepsilon = 3$ and we use the value $\varepsilon = 1$ in the second simulation. In each case we set $\sigma = 1$ in (2.8).

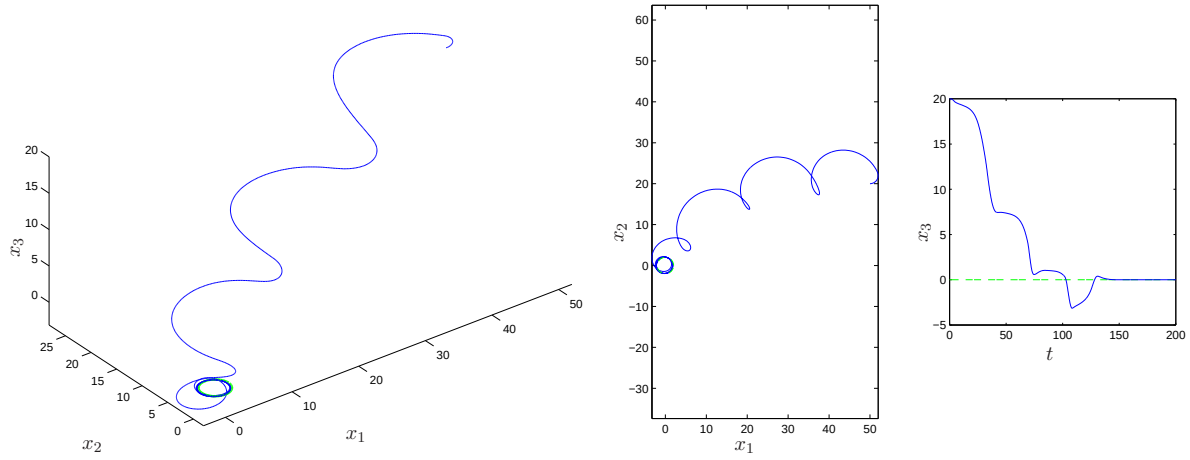

(a) (b)

Figure 2: Illustration of Lyapunov-LaSalle-based 3D-planification results with starting point $(x_{10}, x_{20}, x_{30}) = (50, 20, 20)$, control constraints $u_{1\max} = u_{2\max} = 0.1$, $u_{3\max} = 0.5$, $a_3 = 0.1$, $\sigma = 1$ and $\varepsilon = 3$. (a) The $(x_1(\cdot), x_2(\cdot), x_3(\cdot))$ trajectory, (b) projection in the horizontal plane (left) and evolution of x_3 w.r.t. time (right).

3 The time-optimal stabilizing synthesis

In this section for every $(x_f, y_f, \theta_f) \in \mathbb{R}^2 \times S^1$, we would like to find the control steering (x_f, y_f, θ_f) to the final manifold $\mathcal{C}$ (defined in Section 2.1.1). The collection of all such trajectories is called the *time-optimal stabilizing synthesis*.

Let us again mention the works [1, 43] treating completely the point-to-point time-optimal problem.

It is convenient to change the sign of the dynamics and to consider the equivalent problem of finding the *time-optimal synthesis* issued from $\mathcal{C}$, namely the collection of all time-optimal trajectories starting from $\mathcal{C}$. More precisely we consider the following problem that we shall

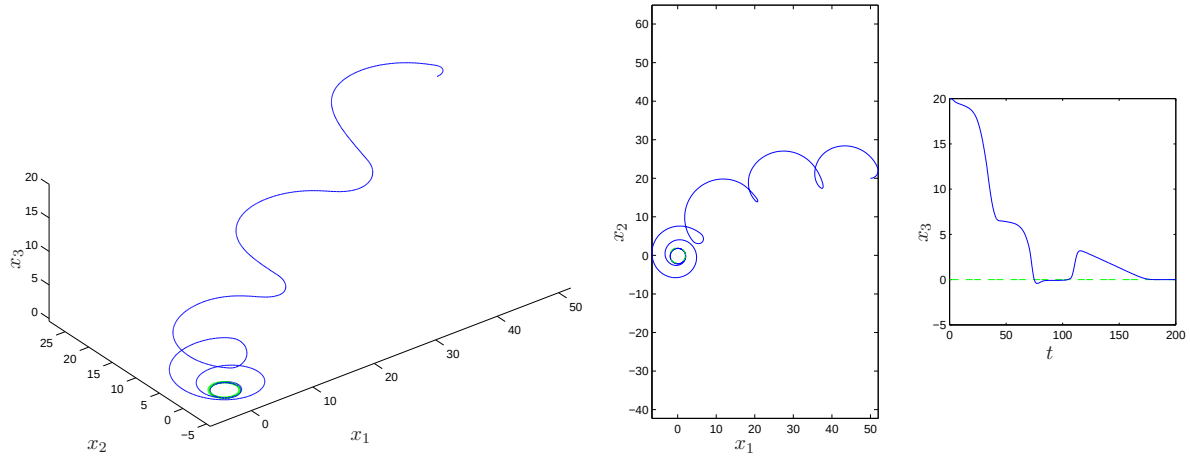

(a)

(b) Projection in the horizontal plan and evolution of x_3 over the time.

Figure 3: Illustration of Lyapunov-LaSalle-based 3D-planification results with $\sigma = 1$ and $\varepsilon = 1$.

denote by **(P)**. In this section, for simplicity in exposition we assume that $[-u_{\max}, u_{\max}] = [-1, 1]$ (cf. Remark 2.1).

(P) For every $(x_f, y_f, \theta_f) \in \mathbb{R}^2 \times S^1$ find the pair trajectory-control joining $\mathcal{C}$ to (x_f, y_f, θ_f), which is time-optimal for the control system

$$\begin{cases} \dot{x} = \cos\theta \\ \dot{y} = \sin\theta \\ \dot{\theta} = u, \quad u \in [-1, 1]. \end{cases} \tag{3.1}$$

Once that Problem **(P)** is solved, then the time-optimal stabilizing synthesis is obtained simply by inverting the arrows of the trajectories of the time-optimal synthesis.

To solve Problem **(P)** it is again convenient to work with the reduced system (2.3) in dimension two. Indeed, in dimension two, a complete theory for finding the time-optimal synthesis exists and will be recalled in the next two sections.

Then, we consider the following problem that we shall denote by **(Q)**.

(Q) For every $(\tilde{x}_f, \tilde{y}_f) \in \mathbb{R}^2$ find the pair trajectory-control joining $q_0 = (0, 1)$ to $(\tilde{x}_f, \tilde{y}_f)$, which is time-optimal for the control system

$$\begin{cases} \dot{\tilde{x}} = -u\tilde{y} + 1 \\ \dot{\tilde{y}} = u\tilde{x} \end{cases}, \quad u \in [-1, 1]. \tag{3.2}$$

3.1 Basic definitions and Pontryagin Maximum Principle

Let M be a n-dimensional connected smooth manifold and let F and G be smooth vector fields on M. Consider the following general control-affine time-optimal problem that we shall denote by **(R)**.

(R) For every q_0 and q_f in M find the pair trajectory-control joining q_0 to q_f, which is time-optimal for the control system

$$\dot{q} = F(q) + uG(q), \quad q \in M, \quad u \in [-1, 1]. \tag{3.3}$$

Definition 3.1 (admissible control/trajectory)**.** An *admissible control* $u(\cdot)$ for the system (3.3) is a measurable function $u(\cdot) : [a, b] \to [-1, 1]$. An *admissible trajectory* is a Lipschitz function $q(\cdot) : [a, b] \to M$ satisfying $\dot{q}(t) = F(q(t)) + u(t)G(q(t))$ a.e. for some admissible control $u(\cdot)$.

In the following we assume that the control system is *complete* i.e., for every measurable control function $u(\cdot) : [a, b] \to [-1, 1]$ and every initial state q_0, there exists a trajectory $q(\cdot)$ corresponding to $u(\cdot)$, which is defined on the whole interval $[a, b]$ and satisfies $q(a) = q_0$.

Thanks to the compactness of the set of controls, the convexity of the set of velocities and the completeness of the control system, Filippov's theorem (see for instance [1]) gives,

Proposition 3.2. *For any pair of points in M, there exists a time-optimal trajectory joining them.*

The main tool to compute time-optimal trajectories is the Pontryagin's Maximum Principle (PMP for short). We refer to [1] for a general version of PMP and also [12] for a version of PMP on two-dimensional manifolds for single input control affine systems. The PMP is a first order necessary condition for optimality.

The following theorem is a version of PMP for control systems of the form (3.3) that we state in our own context only.

Theorem 3.1 (PMP for problem **(R)**)**.** *Consider the control system (3.3). Define for every $(q, p, u) \in T^*M \times [-1, 1]$ the function*

$$H(q, p, u) = \langle p, F(q)\rangle + u \langle p, G(q)\rangle . \tag{3.4}$$

If the pair $(q(\cdot), u(\cdot)) : [0, T] \to M \times [-1, 1]$ is time-optimal then there exists a never-vanishing Lipschitz covector $p(\cdot) : t \in [0, T] \mapsto p(t) \in T^*_{q(t)}M$ and a constant $\lambda \leqslant 0$ such that for a.e. $t \in [0, T]$:

i. $\dot{q}(t) = \dfrac{\partial H}{\partial p}(q(t), p(t), u(t))$,

ii. $\dot{p}(t) = -\dfrac{\partial H}{\partial q}(q(t), p(t), u(t))$,

iii. $H(q(t), p(t), u(t)) = \max\limits_{u\in[-1,1]} H(q, p, u)$,

iv. $H(q(t), p(t), u(t)) + \lambda = 0$.

Remark 3.3. A trajectory $q(\cdot)$ (resp. a pair $(q(\cdot), p(\cdot))$) satisfying the conditions given by the PMP is said to be an *extremal* (resp. an *extremal pair*). An extremal corresponding to $\lambda = 0$ is said to be an *abnormal extremal*, otherwise we call it a *normal extremal*.

3.2 An overview on optimal synthesis on 2D-manifolds

In this section we briefly recall the theory of time-optimal syntheses on 2D-manifolds for systems of the form (3.3), developed by Sussmann, Bressan, Piccoli and Boscain in [11, 13, 35, 44] and rewritten in [12].

This section is written to be as much self-consistent as possible. In the remainder of the section, we assume M to be of dimension two.

3.2.1 Basic definitions

For every coordinate chart on the manifold M it is possible to introduce the following three functions:

$$\Delta_A(q) = \det(F(q), G(q)), \tag{3.5}$$
$$\Delta_B(q) = \det(G(q), [F, G](q)), \tag{3.6}$$
$$f_S(q) = -\frac{\Delta_B(q)}{\Delta_A(q)}. \tag{3.7}$$

The sets $\Delta_A^{-1}(0)$, $\Delta_B^{-1}(0)$ of zeros of Δ_A, Δ_B are respectively the set of points where F and G are parallel, and the set of points where G is parallel to $[F, G]$. These loci are fundamental in the construction of the optimal synthesis. In fact, assuming that they are smooth embedded one dimensional submanifolds of M we have the following:

- on each connected component of $M \setminus (\Delta_A^{-1}(0) \bigcup \Delta_B^{-1}(0))$, every extremal trajectory is bang-bang with at most one switching. Moreover, for every switching of the extremal trajectory the value of the control switches from -1 to $+1$ if $f_S > 0$ and from $+1$ to -1 if $f_S < 0$;
- the support of singular trajectories (i.e., trajectories along which the switching function vanishes identically, see Definition 3.5 below) is always contained in the set $\Delta_B^{-1}(0)$.

Then, the synthesis is built recursively w.r.t. the number of switchings of extremal trajectories, canceling at each step the non optimal trajectories (see [12, Chapter 1]).

In the optimal syntheses some special curves appears, namely:

- Switching curves, i.e., curves made of points where the control switches from $+1$ to -1 or viceversa.
- Singular curves, i.e., curves along which the corresponding switching function (see Definition 3.5 below) is identically zero. For these curves the corresponding control can take values in the interior of $[0, 1]$.
- Cut loci, namely curves made of cut points. Given an admissible curve γ of the control system, defined on $[0, T]$, we say that $t_{\text{cut}} \in (0, T)$ (resp. $\gamma(t_{\text{cut}})$) is a cut time (resp. point) if $\gamma|_{[0,t_{\text{cut}}]}$ is time-optimal and $\gamma|_{[0,t_{\text{cut}}+\varepsilon]}$ is not for every sufficiently small ε.

Remark 3.4. Notice that, although the functions Δ_A and Δ_B depend on the coordinate chart, the sets $\Delta_A^{-1}(0)$, $\Delta_B^{-1}(0)$ and the function f_S do not, i.e., they are intrinsic objects related with the control system (3.3).

We are now interested in determining the extremals. A key role is played by the following:

Definition 3.5 (switching function)**.** Let $(q(\cdot), p(\cdot))$ be an extremal pair. The corresponding switching function is defined as $\phi(t) = \langle p(t), G(q(t))\rangle$.

Notice that $\phi(\cdot)$ is continuously differentiable since $\dot{\phi}(t) = \langle p(t), [F, G](q(t))\rangle$ which is continuous.

Definition 3.6 (bang, singular)**.** Let $q(\cdot)$ be an extremal trajectory defined on the time interval $[a, b]$, and let $u(\cdot) : [a, b] \to [-1, 1]$ be the corresponding control. We say that $u(\cdot)$ is a *bang* control if $u(t) = +1$ a.e. in $[a, b]$ or $u(t) = -1$ a.e. in $[a, b]$. We say that $u(\cdot)$ is *singular* if the corresponding switching function $\phi(t) = 0$ in $[a, b]$. A finite concatenation of bang controls

is called a *bang-bang* control. A *switching time* of $u(\cdot)$ is a time $\tau \in [a,b]$ such that, for every $\varepsilon > 0$, $u(\cdot)$ is not bang or singular on $(\tau-\varepsilon, \tau+\varepsilon)\bigcap[a,b]$. An extremal trajectory of the control system (3.3) is called a bang extremal, singular extremal, bang-bang extremal respectively, if it corresponds to a bang control, singular control, bang-bang control respectively. If τ is a switching time, the corresponding point $q(\tau)$ on the trajectory $q(\cdot)$ is called a *switching point.*

The switching function is important because it determines where the controls may switch. In fact, using the PMP, one easily gets:

Proposition 3.7. *A necessary condition for a time τ to be a switching time is that $\phi(\tau) = 0$. Therefore, on any interval where ϕ has no zeros (respectively finitely many zeros), the corresponding control is bang (respectively bang-bang). In particular, $\phi > 0$ (resp. $\phi < 0$) on $[a,b]$ implies $u = 1$ (resp. $u = -1$) a.e. on $[a,b]$. On the other hand, if ϕ has a zero at τ and $\dot{\phi}(\tau)$ is different from zero, then t is an isolated switching.*

3.2.2 More on singular extremals and predicting switchings for 2D-systems

In this section we compute the control corresponding to singular extremals and we would like to predict which kind of switchings can happen, using properties of the vector fields F and G. The following lemmas illustrate the role of the set $\Delta_B^{-1}(0)$ in relation with singular extremals. Proofs can be found in [11, 12, 35].

We denote by $\mathrm{Supp}\,(q(\cdot))$ the support of the trajectory $q(\cdot)$.

Lemma 3.8. *Let $q(\cdot)$ be an extremal trajectory which is singular on a time interval $[a,b]$ included in the domain of $q(\cdot)$. Then, $q(\cdot)|_{[a,b]}$ corresponds to the so-called singular control $\varphi(q(t))$, where*

$$\varphi(q) = -\frac{\Delta_{B*q}\,(F(q))}{\Delta_{B*q}\,(G(q))}, \tag{3.8}$$

with Δ_A and Δ_B defined in equations (3.5) and (3.6) and Δ_{B*q} being the tangent map of Δ_B at point q. Moreover, on $\mathrm{Supp}\,(q(\cdot))$, $\varphi(q)$ is always well-defined and its absolute value is smaller or equal to one. Finally $\mathrm{Supp}\,(q(\cdot)|_{[a,b]}) \subset \Delta_B^{-1}(0)$.

The following lemma describes what happens when Δ_A and Δ_B are different from zero.

Lemma 3.9. *Let $\Omega \subset M$ be an open set such that $\Omega\bigcap(\Delta_A^{-1}(0)\bigcup\Delta_B^{-1}(0)) = \emptyset$. Then all connected components of $\mathrm{Supp}\,(q(\cdot))\bigcap\Omega$, where $q(\cdot)$ is an extremal trajectory of (3.3), are bang-bang with at most one switching. Moreover, if $f_S|_\Omega > 0$, then $q(\cdot)|_\Omega$ is associated to a constant control equal to $+1$ or -1 or has a switching from -1 to $+1$. If $f_S|_\Omega < 0$, then $q(\cdot)|_\Omega$ is associated to a constant control equal to $+1$ or -1 or has a switching from $+1$ to -1.*

Remark 3.10. For the problem **(R)**, under generic conditions on the vector fields F and G, one can make the complete classification of synthesis singularities, stable synthesis, singularities of the minimum time wave fronts. We refer to [12] for the general theory. For some extensions to higher dimension, see [2, 40].

3.3 Construction of the time-optimal stabilizing synthesis for the reduced system

Let us apply the theory of the previous section to problem **(Q)**.

3.3.1 Preliminary observations

Define

$$F = \begin{pmatrix} -1 \\ 0 \end{pmatrix}, \quad G = \begin{pmatrix} \tilde{y} \\ -\tilde{x} \end{pmatrix}, \quad Y = F + G = \begin{pmatrix} -1 + \tilde{y} \\ -\tilde{x} \end{pmatrix}, \quad X = F - G = \begin{pmatrix} -1 - \tilde{y} \\ \tilde{x} \end{pmatrix}.$$

The integral curves of the vector fields Y and X are shown below (Fig. 4).

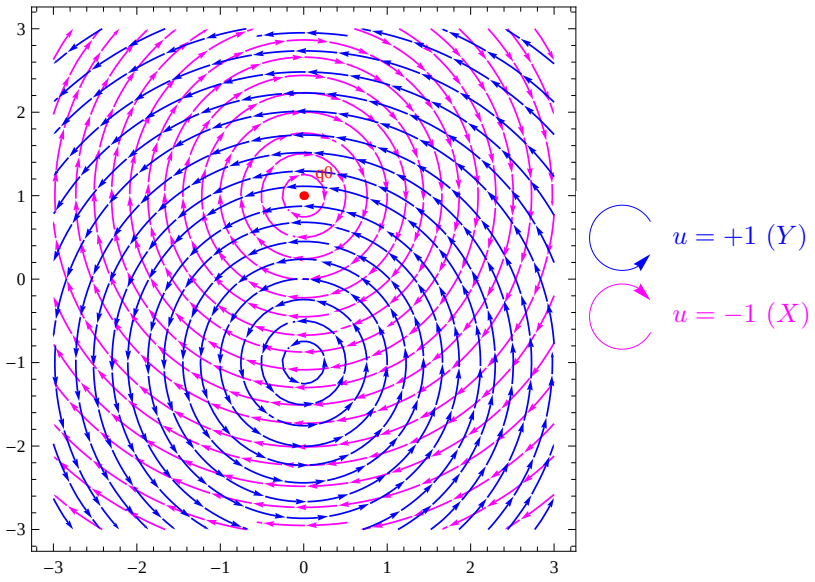

Figure 4: Integral curves of projected X and Y

We compute the quantities,

$$\begin{aligned} \Delta_A(\tilde{x}, \tilde{y}) &= \det(F(\tilde{x}, \tilde{y}), G(\tilde{x}, \tilde{y})) = \det \begin{pmatrix} -1 & \tilde{y} \\ 0 & -\tilde{x} \end{pmatrix} = \tilde{x}, \\ \Delta_B(\tilde{x}, \tilde{y}) &= \det(G(\tilde{x}, \tilde{y}), [F, G](\tilde{x}, \tilde{y})) = \det \begin{pmatrix} \tilde{y} & 0 \\ -\tilde{x} & 1 \end{pmatrix} = \tilde{y}, \\ f_S(\tilde{x}, \tilde{y}) &= -\frac{\Delta_B(\tilde{x}, \tilde{y})}{\Delta_A(\tilde{x}, \tilde{y})} = -\frac{\tilde{y}}{\tilde{x}}. \end{aligned}$$

Using Lemmas 3.8 and 3.9 it follows that:

- on the set $\{\tilde{x} > 0\} \bigcap \{\tilde{y} > 0\}$ only the switching from $+1$ to -1 is allowed. And cyclically on the other quadrants.
- If there are singular trajectories then they should lie on the set $\{\tilde{y} = 0\}$. Notice that a trajectory whose support is $\{\tilde{y} = 0\}$ [2] is admissible (it corresponds to the zero control). See Fig. 5.

[2] According to [12], the set $\{\tilde{y} = 0\}$ is a turnpike (i.e., a trajectory that is locally time-optimal)

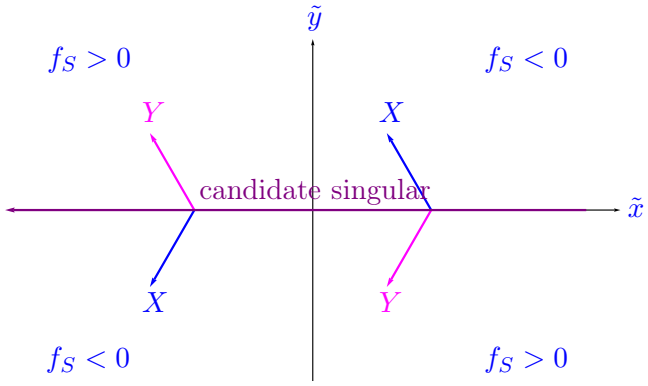

Figure 5: Candidate singular

We construct the time-optimal synthesis in the following way:

- STEP 0. We consider the trajectory γ^- starting from q_0 with control -1. All extremal trajectories should start in this way since in a neighborhood V of q_0 we have that $f_S < 0$ and hence neither singular trajectories nor trajectories having chattering could be extremal in V. Moreover, a trajectory cannot start from q_0 with control $+1$ since the vector field $Y(q_0) = 0$.
- STEP 1. We compute the last time at which the trajectory γ^- is extremal (or has lost optimality because it self-intersects) and we study which kind of extremal trajectories can bifurcate from γ^-.
- STEP 2. For each bang or singular trajectory bifurcating from γ^-, we study the last time at which it is extremal. If there are intersections among trajectories, we cancel those parts that are not optimal (among trajectories already computed up to this step).
- STEP 3. For each trajectory γ defined on $[0, \tau_\gamma]$ computed at the previous step do the following. If at τ this trajectory looses optimality (among trajectories of the previous step), do nothing otherwise prolong γ with the next bang or singular trajectory up to the last time at which it is extremal. If there are intersections among trajectories, cancel those parts that are not optimal (among trajectories already computed up to this step). Notice that in general there could be several prolongations of γ that are extremal. Hence, in general, new extremal trajectories are generated at this step.

Then, the synthesis is built recursively, repeating STEP 3 up to when no new trajectories are generated. Notice that a trajectory generated at STEP n has n concatenations of bang or singular trajectories. In our case, only one application of STEP 3 is necessary.

3.3.2 Adjoint equation

To compute the last time at which bang and singular trajectories are extremal, we need the adjoint equation. From equation (3.4) we have that $H(\tilde{x}, \tilde{y}, \xi, \zeta, u) = -\xi + u(\xi\tilde{y} - \zeta\tilde{x})$ (here $q = (\tilde{x}, \tilde{y})$ and $p = (\xi, \zeta)$). Hence,

$$\begin{cases} \dot{\xi} = u(t)\zeta \\ \dot{\zeta} = -u(t)\xi. \end{cases} \tag{3.9}$$

3.3.3 STEP 1: Analysis along the curve starting from q_0 and corresponding to control -1

The trajectory γ^- starting from q_0 and corresponding to control -1 has coordinates:

$$\begin{aligned}\tilde{x}^-(t) &= -2\sin(t)\\ \tilde{y}^-(t) &= 2\cos(t) - 1\end{aligned}$$

This curve intersects the $\tilde{x}$-axis at time $t_1 = \pi/3$. The solution of the adjoint equation with $u = -1$ and the normalization $|p(0)| = 1$ is,

$$\begin{aligned}\xi(t,\alpha) &= \cos(t+\alpha)\\ \zeta(t,\alpha) &= \sin(t+\alpha),\end{aligned}$$

where α is defined by $\cos(\alpha) = \xi(0)$, $\sin(\alpha) = \zeta(0)$. Notice that the condition $H + \lambda = -\xi + u(\xi\tilde{y} - \zeta\tilde{x}) + \lambda = 0$ with $\lambda \leqslant 0$, written at the initial point implies that,

$$-\cos(\alpha) + u\cos(\alpha) = \cos(\alpha)(u-1) \geqslant 0.$$

Since we start with control -1 we have that $\alpha \in [\pi/2, 3/2\pi]$.

Then, the switching function is given by

$$\phi_\alpha(t) = p(t)G(\gamma^-(t)) = 2\cos(\alpha) - \cos(t+\alpha).$$

By studying this function it follows that:

- for $\alpha = \pi/2$, ϕ_α starts with value zero and then takes positive values: it cannot correspond to a trajectory starting with control -1.
- For $\alpha \in (\pi/2, 2\pi/3)$, ϕ_α starts with negative values, and has its first zero (of order one) (close to the origin for values of α close to $\pi/2$). For every $\tau \in (0, \pi/3)$ there exists a unique $\alpha \in (\pi/2, \pi/3)$ for which the switching function has a zero at τ.
- For $\alpha = 2\pi/3$, ϕ_α starts with negative values and has a double zero at $t = \pi/3$ (the point q_S at which the trajectory meets the turnpike). Notice that there exists an extremal trajectory entering the turnpike, since there is a trajectory switching there (see the singularity (Y, S) in [12, page 62]).
- For $\alpha \in (2\pi/3, 4\pi/3)$, ϕ_α is always negative. This means that the trajectory with control -1 is always extremal (a priori, γ^- can make many turns !).
- For $\alpha = 4\pi/3$, ϕ_α starts with negative values and has a double zero at $t = 5\pi/3$ (again at a point $\bar{q}_S$ where the trajectory meets the turnpike). Again notice that there exists an extremal trajectory entering the turnpike, since there is a trajectory switching there.
- For $\alpha \in (4\pi/3, 3\pi/2)$, ϕ_α starts with negative values, and then has its first zero (of order one) (close to $t = 5\pi/3$ for small values of α close $4\pi/3$). For every $\tau \in (\pi, 5\pi/3)$ there exists a unique $\alpha \in (4\pi/3, 3\pi/2)$ for which the switching function has a zero at τ.
- For $\alpha = 3\pi/2$, ϕ_α starts with negative values, and has its first zero (of order one) at $t = \pi$.

This study being done, we get the expression of the first switching time τ_1 solving the equation $\phi_\alpha(\tau_1) = 0$ (and taking into account that $\tau_1 > 0$). It yields

$$\tau_1(\alpha) = -\alpha + \arccos(2\cos\alpha), \quad \alpha \in \left(\frac{\pi}{2}, \frac{2\pi}{3}\right] \bigcup \left[\frac{4\pi}{3}, \frac{3\pi}{2}\right]. \tag{3.10}$$

Notice that γ^- is extremal for every $t > 0$. However, γ^- cannot be optimal after $t = 2\pi$ since it is periodic.

The initial conditions of the covector are shown below (Fig. 6).

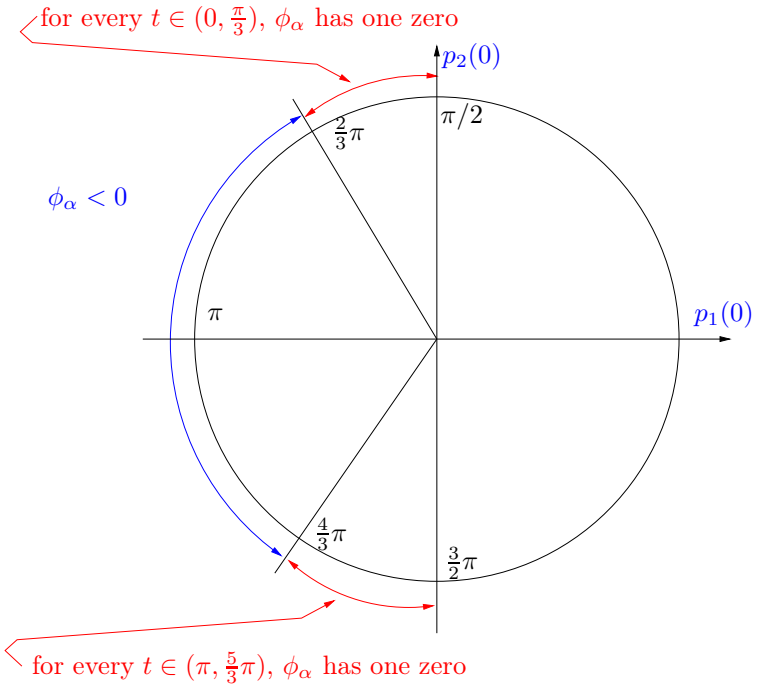

Figure 6: Initial conditions of covector

3.3.4 STEP 2

At this step we study separately the following four families of trajectories bifurcating from γ^-.

- Family 1: trajectories bifurcating from $\gamma^-[0, \pi/3)$.
- Family 2: the singular trajectory bifurcating from $q_S = \gamma^-(\pi/3) = (-\sqrt{3}, 0)$.
- Family 3: trajectories bifurcating from $\gamma^-[\pi, 5/3\pi]$
- Family 4: the singular trajectory bifurcating from $\bar{q}_S = \gamma^-(5\pi/3) = (\sqrt{3}, 0)$

The extremal trajectories bifurcating from γ^- are drawn in the following picture (Fig. 7).

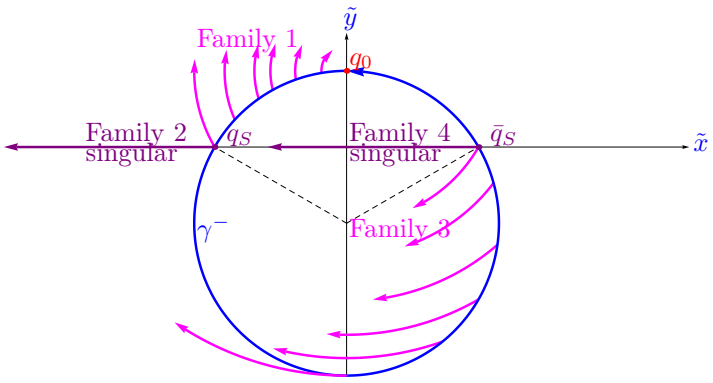

Figure 7: Extremal trajectories bifurcating from γ^-

Family 1. Consider a curve corresponding to control $+1$ starting from the point $\gamma^-(\tau_1)$, with $\tau_1 = \tau_1(\alpha)$, $\alpha \in [\pi/2, 2\pi/3]$ (which corresponds to $\tau_1 \in [0, \pi/3]$). Its coordinates are:

$$\begin{aligned} x(t,\tau_1) &= 2\sin(t-\tau_1) - 2\sin(t) \\ y(t,\tau_1) &= 1 - 2\cos(t) + 2\cos(t-\tau_1) \end{aligned}$$

The corresponding covector which satisfies the switching condition at the beginning

$$p(0,\tau_1)G(x(0,\tau_1), y(0,\tau_1)) = 0,$$

has coordinates

$$\begin{aligned} \xi(t,\tau_1) &= \cos(t-\tau_1-\alpha) \\ \zeta(t,\tau_1) &= -\sin(t-\tau_1-\alpha), \end{aligned}$$

The switching function is given by (here we have taken account that $\phi_\alpha(\tau_1) = 0$)

$$\tilde{\phi}_\alpha(t+\tau_1) = \cos(t-\tau_1-\alpha) - 2\cos(\alpha).$$

We get the expression of the second switching time τ_2 solving the equation $\tilde{\phi}_\alpha(\tau_2+\tau_1) = 0$ (and taking into account that $\tau_2 > 0$). It yields

$$\tau_2(\alpha) = 2\arccos(2\cos\alpha), \quad \alpha \in \left(\frac{\pi}{2}, \frac{2\pi}{3}\right]. \tag{3.11}$$

The switching curve is shown in the following picture (Fig. 8).

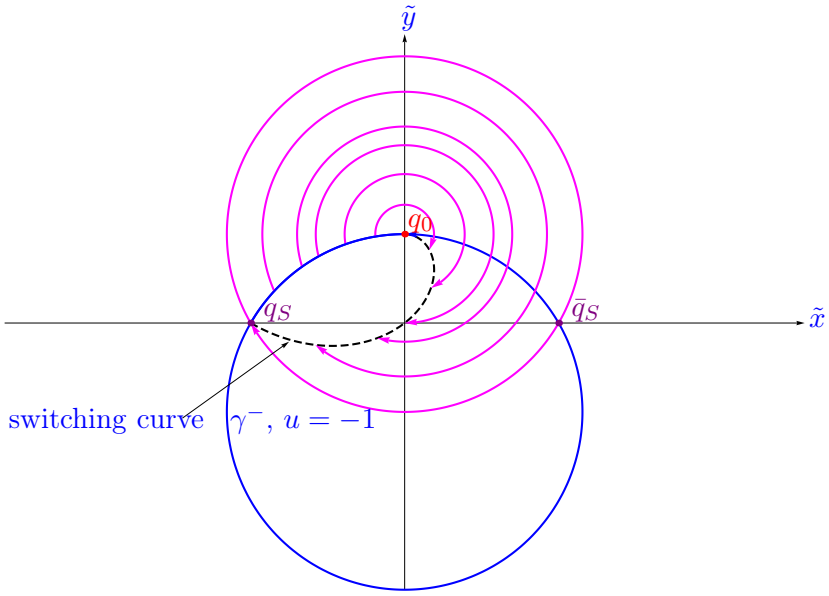

Figure 8: Switching curve family 1

Family 2: the singular trajectory. Since there is a trajectory switching from γ^- in q_S it follows that there exists an extremal trajectory entering the turnpike. At the entrance point of the turnpike the covector satisfies $\langle p_S, G(q_S)\rangle = 0$. Since $G = (y, -x)$ it follows that $\langle p_S, (0, \sqrt{3})\rangle = 0$. Hence we can assume that

$$p_S = (-1, 0).$$

The minus sign has been chosen in such a way that $\langle p_S, F + uG\rangle \geqslant 0$ (according to Theorem 3.1, $H + \lambda = \langle p_S, F + uG\rangle + \lambda = 0$, with $\lambda \leqslant 0$). On the singular trajectory the control can be only zero. From equation (3.9) it follows that p is constant. Hence the singular trajectory is extremal for all positive times (Fig. 9).

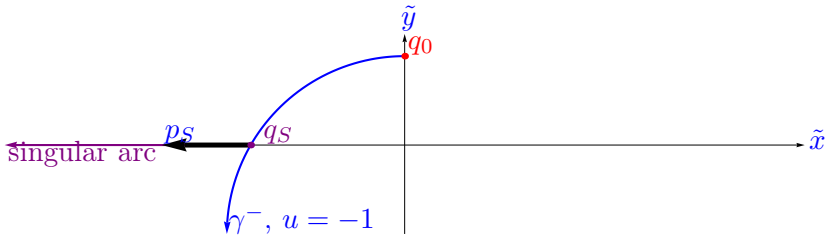

Figure 9: Singular arc

Family 3. This family is treated exactly as Family 1. The only difference is that now $\alpha \in [4\pi/3, 3\pi/2]$ (which corresponds to $\tau_1 \in [\pi, 5\pi/3]$). The switching curve is shown on the following picture (Fig. 10).

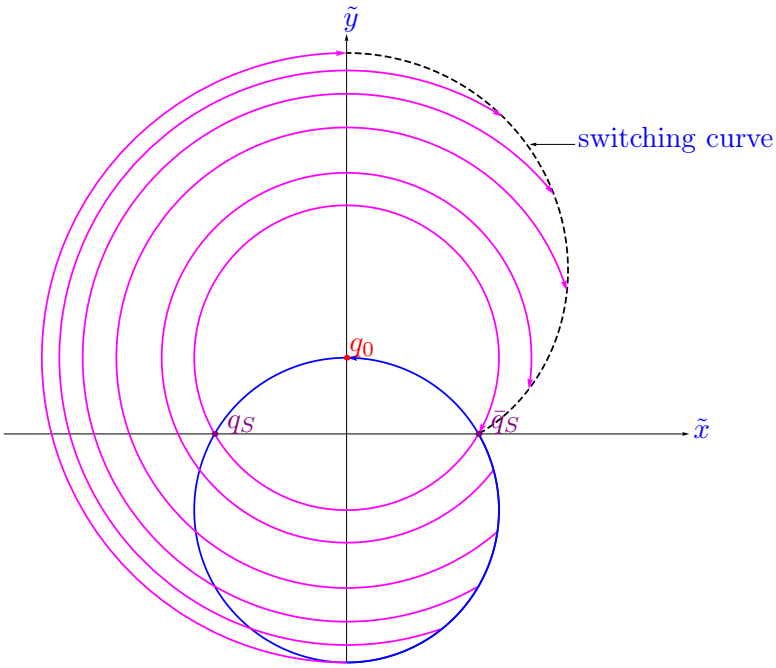

Figure 10: Switching curve family 3

Family 4. This family is treated exactly as Family 2. Since there is a trajectory switching from γ^- at $\bar{q}_S$ it follows that there exists an extremal trajectory entering the turnpike. This trajectory is then extremal for every positive time (Fig. 11).

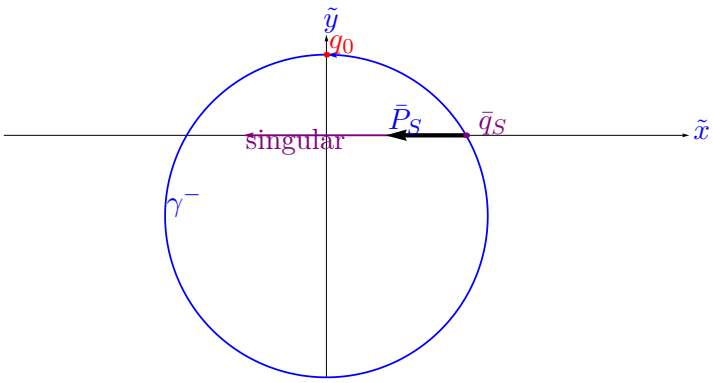

Figure 11

Cutting non optimal trajectories. A direct computation yields the following.

- The trajectory γ^- is not optimal after passing through the point $\bar{q}_S$.
- Let us call γ_{crazy} the trajectory of Family 3 corresponding to $\tau_1 = \pi$ (i.e., $\alpha = 3\pi/2$). This trajectory is not optimal after crossing the singular trajectory of Family 2.
- The trajectories of Family 3 for $\tau_1 \in (\pi, 5\pi/3)$ (i.e., $\alpha \in (4\pi/3, 3\pi/2)$) are not optimal after crossing the γ^- trajectory.
- Let us call γ_{double} the trajectory of Family 3 corresponding to $\tau_1 = 5\pi/3$ (i.e., $\alpha = 4\pi/3$). This trajectory is not optimal after passing through the point q_S. Notice that the support of this trajectory coincides with part of the support of a trajectory of Family 1 (the one corresponding to $\tau_1 = \pi/3$ (i.e., $\alpha = 2\pi/3$).

- The singular trajectory of Family 4 is not optimal.

It follows that only the trajectories shown in the following picture are candidates to be optimal. These are the trajectories generated at STEP 2 (Fig. 12).

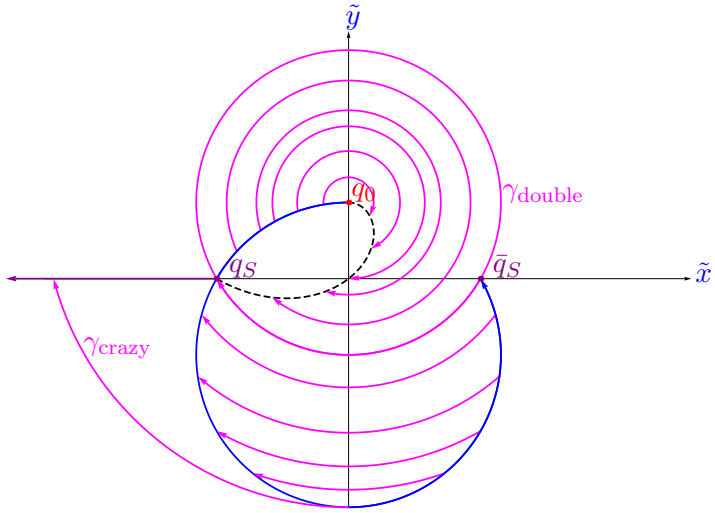

Figure 12: Trajectories generated at STEP 2

3.3.5 STEP 3

The trajectories generated at this step are shown on the following figure where they are divided in four families: family 2.1, 2.2, 2.3 and 2.4 (Fig. 13).

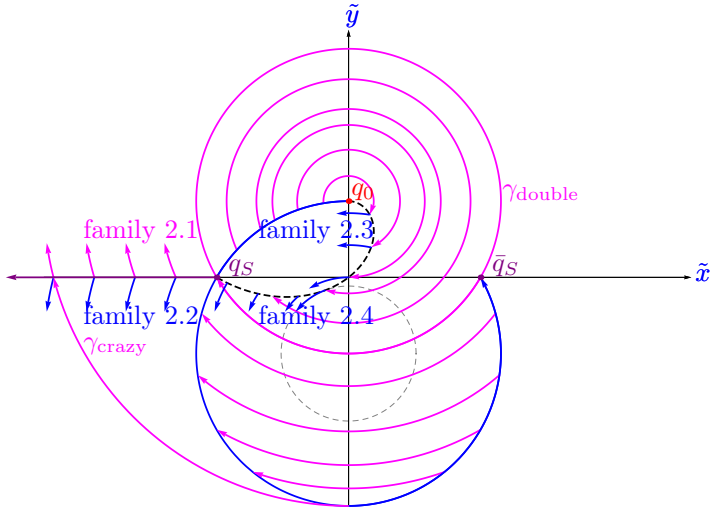

Figure 13: Trajectories generated at STEP 3

The point $\bar{q}_{\text{top}}$ that divides the families 2.3 and 2.4 is the point at which the switching curve generated at the previous step become tangent to an integral curve of the vector field X.

The coordinates of the point $\bar{q}_{\text{top}}$ are $\left(-\sqrt{\frac{59\sqrt{3}}{2} - 51}, \frac{1}{2}\left(5\sqrt{3} - 9\right) \right)$.

Remark 3.11. Notice the following important fact. The trajectory of Family 1 of STEP 1 corresponding to $\alpha = \arccos\left(-\sqrt{5}/4\sqrt{2}\right)$ (i.e., $\tau_1 = 2\arcsin(1/4)$ and $\tau_2 = 3\pi/2 + \arcsin(1/4)$) has a switching at the origin at time $t = 3\pi/2 + 3\arcsin(1/4)$. However, this trajectory cannot

be connected to a singular trajectory. This is due to the fact that the vector field G is zero at this point. Hence, the switching function vanishes but the covector has not necessary the right direction to make the trajectory enter the turnpike extremal. This phenomenon is similar to the one described in [10, Fig. 4.6]. A direct computation shows that the value of the covector of this trajectory at the origin is $\left(-\sqrt{5/8}, \sqrt{3/8}\right)$ while a covector of the form $(-1, 0)$ is necessary to enter the turnpike.

We have the following

- The family 2.4 is clearly not optimal since it is generated by a switching curve that *reflects* the trajectories (see the analysis of $\bar{C}$ curves in [12, §4.1.3]).
- The families 2.1 and 2.2 do not stop to be extremal before meeting the set $\mathcal{K}_1 = \{(x, 0) | x > \sqrt{3}\}$. This set is a cut locus. The curve γ_{crazy} is not optimal. It is quicker to take trajectories from the family 2.2.
- The family 2.3 loses optimality when it meets Family 3 of the previous step. It forms then a cut locus $\mathcal{K}_2$ which is a one-dimensional manifold starting from $\bar{q}_{\text{top}}$ and arriving to a point q_{bottom} on the γ^- trajectory. The coordinates of the point q_{bottom} are $\left(-\sqrt{3}, -2\right)$.

  This cut locus has the following features:

  - at $\bar{q}_{\text{top}}$ it is C^1-connected to the switching curve from which the family 2.3 is generated. This tangency is a consequence of the general theory developed in [12]. It is called a $(C, K)_2$ singularity (see [12, Fig. 2.21]).
  - It is not smooth at one point that we denote by $\bar{q}_{\text{middle}}$. More precisely, it is not smooth at the intersection with the curve γ_{double} that separates the families 1 and 3 of the previous STEP. The presence of this nonsmoothness point is a consequence of the fact that the minimum-time front is not smooth along the curve γ_{double}. Indeed this trajectory separates two different families.

    The coordinates of the point $\bar{q}_{\text{middle}}$ are $\left(-\frac{\sqrt{15}}{4}, -\frac{3}{4}\right)$.
  - At the point q_{bottom} it is C^1-connected to the curve γ^-. This fact is the consequence of the tangency of Family 3 with γ^- at the point $\gamma^-(\pi)$.

Since all the trajectories generated at this step are either defined on $[0, +\infty)$ or on $[0, T]$ with cut time T, it follows that no new trajectories are generated at subsequent steps. Hence, the time-optimal synthesis is constructed (Fig. 14).

Remark 3.12. Notice that the minimum time function is not continuous on $\gamma^-([0, \pi))$.

As a consequence, the optimality of the synthesis cannot be confirmed a posteriori using the verification theorem ([36, Theorem 2.13]) based on the notion of regular synthesis as it was done in [42] for the case of the Dubins' system for tracking a rectilinear route in minimum time. Indeed, it is easy to see that the minimum time function is not weakly upper semicontinuous (w.u.s.c. for short) and thus does not match the hypothesis of [36, Theorem 2.13]. To see this let $q_n \to q_0$ as $n \to \infty$ with q_n belonging to the switching curve. Denote by $V(q)$ the minimum time to reach q_0 from q. We have $V(q_0) = 0$ and according to (3.10) and (3.11) $V(q_n) = -\alpha_n + 3 \arccos(2 \cos \alpha_n)$ where $\alpha_n \to \pi/2$ as $n \to \infty$. But $\lim_{n \to \infty} V(q_n) = \pi > 0 = V(q_0)$ which shows that V is not w.u.s.c. at q_0.

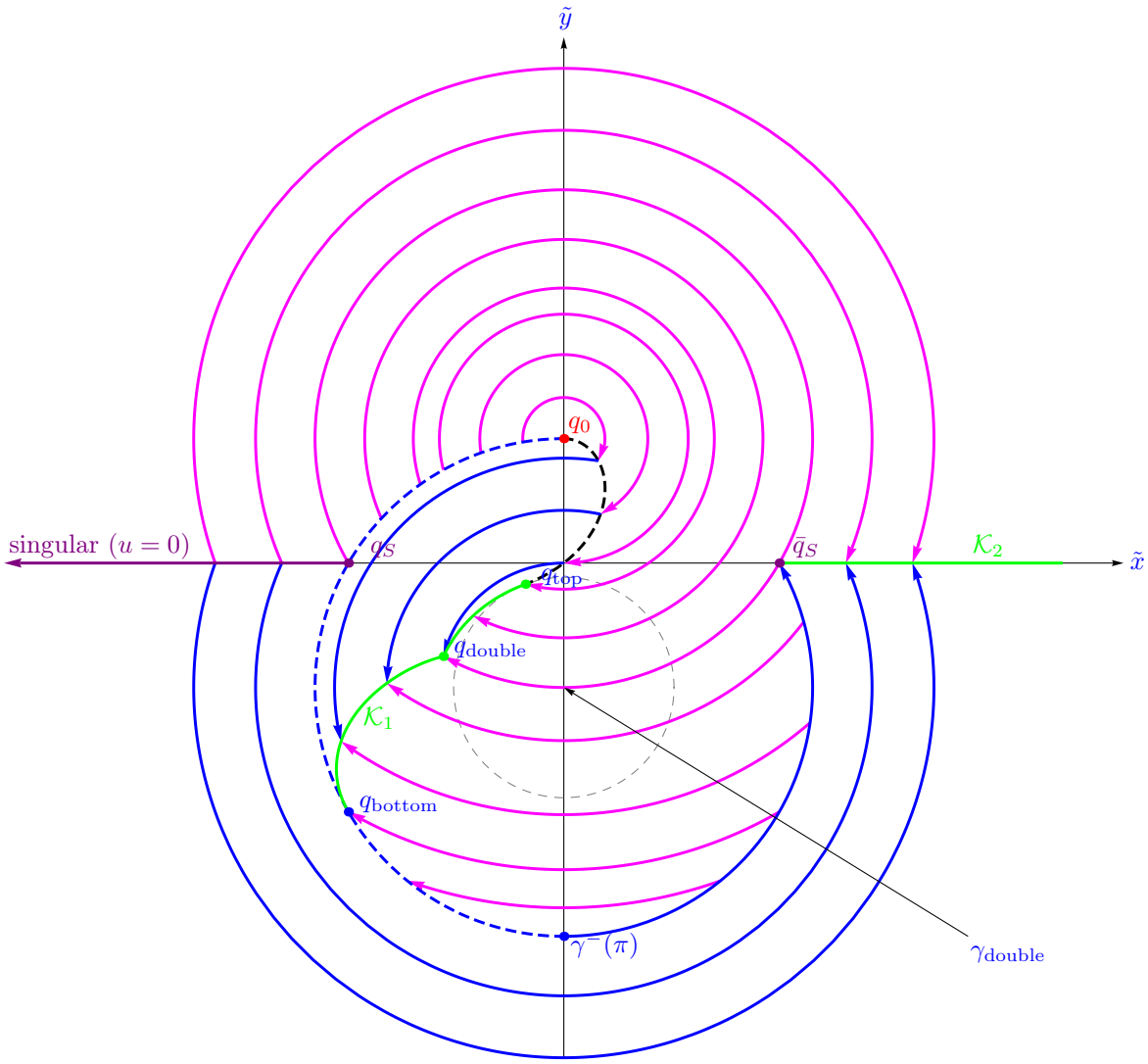

Figure 14: The projected optimal synthesis

3.4 Correspondance between the solutions to problem (P) and problem (Q)

The solutions to problem **(P)** can be deduced from the solutions to problem **(Q)**. In this section we display pairs of figures showing a solution of problem **(P)** and its corresponding lifted solution to problem **(Q)**. Pictures are shown for each type of solution: bang-bang, bang-bang-bang, and bang-singular-bang trajectories.

Let us make a few remark on the time-optimal synthesis of problem **(P)**.

As the reader can easily check using a similar argument as it was done in [42], the application of PMP to problem **(P)** leads to the following lemma describing some of the feature of the synthesis.

Lemma 3.13. *Optimal paths solving Problem* **(P)** *are such that rectilinear segments and points of inflection belong to a same line passing through the center of the final manifold* $\mathcal{C}$.

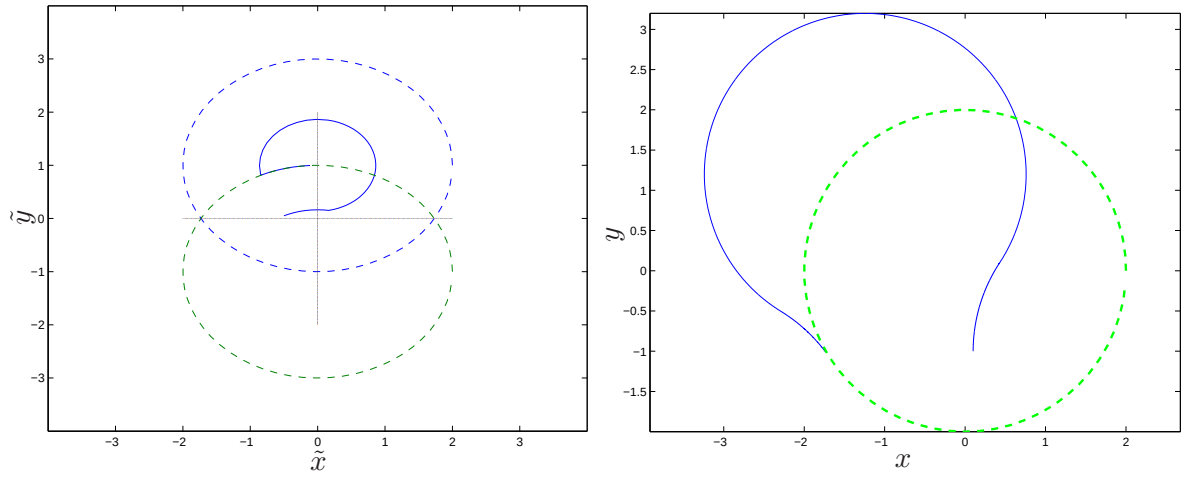

Figure 15: A bang-bang-bang optimal trajectory. A bang-bang-bang solution to problem **(Q)** (left) and the corresponding optimal solution to problem **(P)** (right).

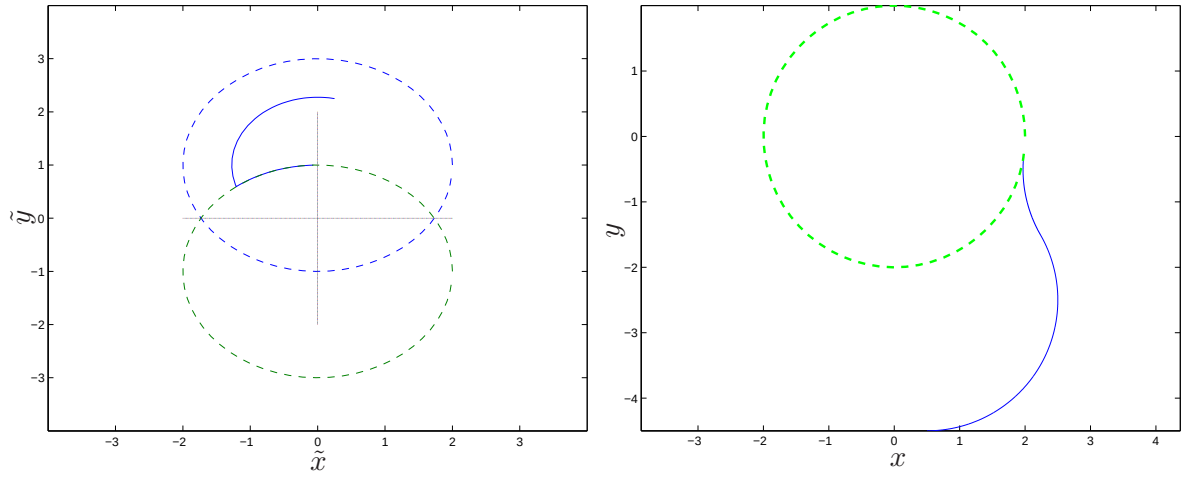

Figure 16: A bang-bang optimal trajectory. A bang-bang solution to problem **(Q)** (left) and the corresponding optimal solution to problem **(P)** (right).

4 Tracking a moving target

The steering methods presented in the previous sections of this paper were concerned with a fixed target . In this section, the results of the previous sections are brought together for the development of a control strategy for tracking a moving target .

This tracking problem has been tackled in different ways. For instance, while some authors use predefined pieces of trajectories called *patterns* that depend on the difference of velocity between the target and the UAV [29, 33] some others prefer to use some simple algorithm based on tangent vector or lateral guidance laws [38, 45] in order to compute in real time the desired path for the UAV. Some authors consider that the tracking problem can be modeled by a predator-prey model which gives waypoints to be interpolated by the UAV [4].

Also, some authors use the same kind of methods as the ones we have described in the previous sections. For instance, in [32] a method using "Lyapunov vector fields" is presented to track a moving target .

Time-optimal problem to manage convoy protection has been considered in [20] where the

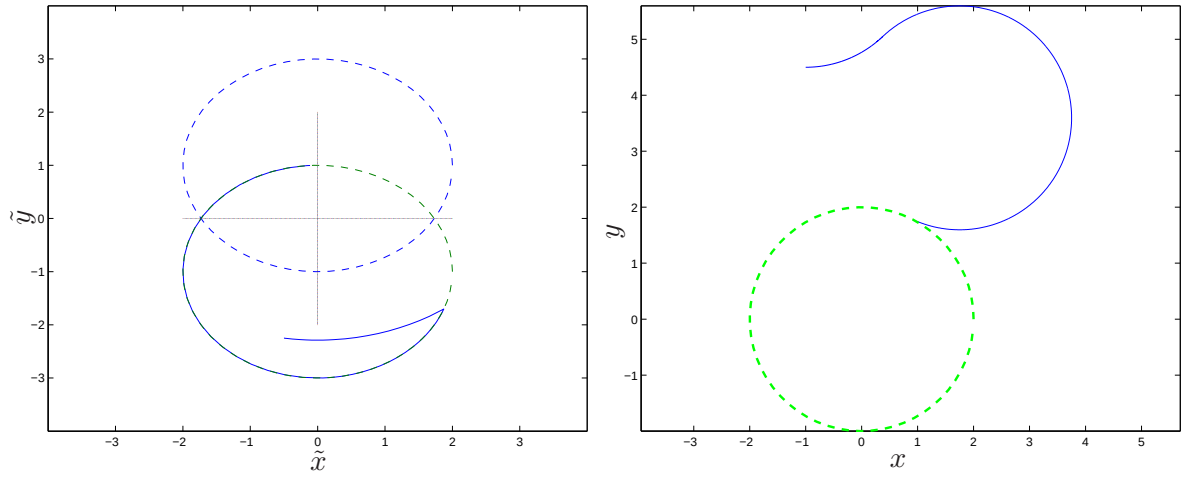

Figure 17: Another bang-bang optimal trajectory. A bang-bang solution to problem **(Q)** (left) and the corresponding optimal solution to problem **(P)** (right).

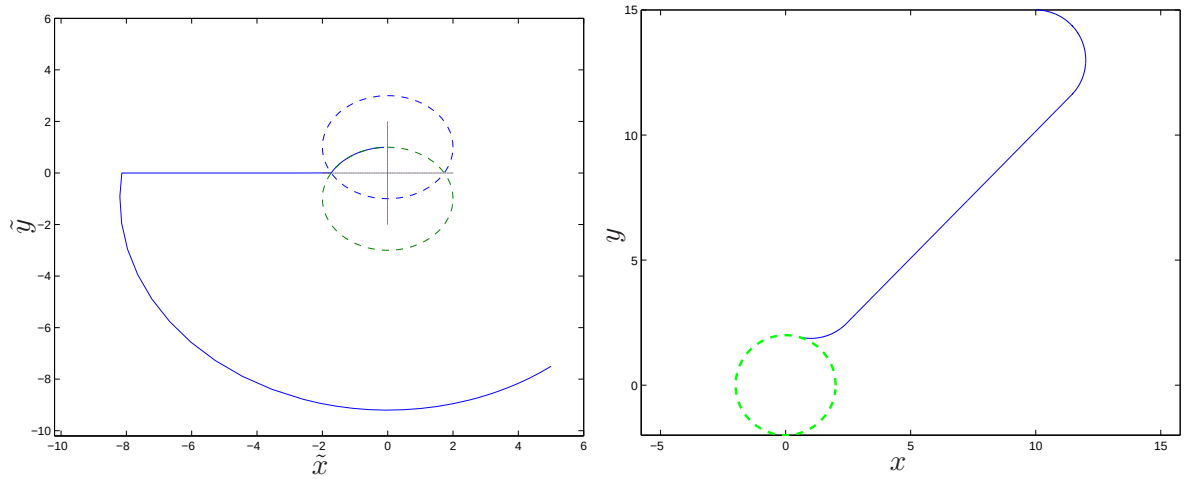

Figure 18: A bang-singular-bang optimal trajectory. A bang-singular-bang solution to problem **(Q)** (left) and the corresponding optimal solution to problem **(P)** (right).

authors consider that the minimum turning radius of UAV is greater than the radius of the protection circle around the target , i.e., the UAV cannot follow this circular trajectory.

4.1 Statement of the problem

Our goal is to make the UAV reach and track a time-parameterized circular final manifold $\mathcal{C}_t$ lying in an horizontal plane above the moving target . Both cases when the future trajectory of the target is known or not are considered.

Let $z = (z_1, z_2, z_3)$ represent the target coordinate in $\mathbb{R}^3$. Define $\mathcal{C}_t$ to be the time-parameterized counterclockwise oriented circle with minimal turning radius $r = 1/u_{\max}$ centered at $(z_1(t), z_2(t))$ in a horizontal plane of a given altitude above the target .

The simple algorithm presented below depicts an open-loop controller which can be used in a high-level controller that is itself used to find waypoints to be sent to the low-level controller performing the closed-loop control of the UAV.

Here for every position of a HALE or MALE UAV, modeled by (2.1) or (2.5) respectively,

we would like to find a trajectory steering the considered UAV to the minimum curvature horizontal circle centered at the centroid of a moving target , at a given altitude w.r.t. the target .

It is necessary to make some assumptions on the target behavior. First, we assume that the target speed v_{target} is smaller than the UAV speed v_{uav}, since it is clear that without this assumption the UAV cannot follow the target .

Summing up we consider the following problem

Problem T *Given two initial conditions $z(0) = z_0$ and $q(0) = q_0$ in the corresponding state spaces of the target and the considered UAV, find a pair trajectory-control joining q_0 to $\mathcal{C}_t$ which is admissible for the considered control system.*

4.2 Description of the algorithm

We assume that the past behaviors of both the UAV and the target are known. In practice, the target trajectory is obtained via an external module (as for example a vision based module see [22]).

The following rough algorithm describes a high-level open-loop target tracking controller. We construct the path in the following way

- **STEP 0.** Acquisition of initial data $z_0 \in \mathbb{R}^3$ and $q_0 \in \mathbb{R}^3 \times SO(3)$, the position of the target and UAV respectively.

  Set $t = 0$.
- **STEP 1.** Compute $t^* = \min\{s \in \mathbb{R}_+ \mid q(t+s) \in \mathcal{C}_t)\}$.
- **STEP 2.** Predict the value of $z(t + t^*)$.
- **STEP 3.** Compute the pair trajectory-control $(q(\cdot), u(\cdot))$ to reach the $\mathcal{C}_{t+t^*}$ and apply the control to the UAV.
- **STEP 4.** Set $t = t + \Delta t$ and go to STEP 1, where Δt is some time step, that may either be constant or actualized in terms of external informations.

Remark 4.1. There is of course no convergence result for this strategy. Here, we just give an idea on how to apply our previous steering methods in the case of a moving target . Of course the positioning error occurring at **STEP 3** of the previous algorithm should be studied.

Remark 4.2 (more precisions on the different steps of the algorithm)**.**
-At **STEP 1** we compute the final time t^* to reach the $\mathcal{C}_t$. Depending on the method, the value of this final time will be obtained exactly or not. The time-optimal method yields the exact time to reach the final manifold $\mathcal{C}_t$. In this case, t^* is solution to problem **(P)** (or **(Q)**, see Section 3). When the Lyapunov method is used, $\mathcal{C}_t$ is reached asymptotically and the time t^* is the first positive time at which the UAV enters a neiborhood $\mathcal{C}_t^\varepsilon = B(z(t), r+\varepsilon) \bigcap B(z(t), r-\varepsilon)$ of $\mathcal{C}_t$. The parameters ε can then be tuned in order to improve on the performance of the path following algorithm.

-At **STEP 2** we make a prediction of the future position (in space) $z(t+t^*)$ of the target . Of course this position may be obtained in different manners. The method we have used consists of using an observer in order to reconstruct the target velocities. In this work we implemented

the so-called extended Kalman filter (EKF for short) (see e.g. [6, 41, 37]) which is well-known for its robustness w.r.t. the noise.

For this purpose, let us assume that the target dynamics is also modeled by an extended Dubins system (see [17])

$$\begin{cases} \dot{z}_1 = u_1 \cos\theta \\ \dot{z}_2 = u_1 \sin\theta \\ \dot{z}_3 = u_2 \\ \dot{\theta} = u_3, \end{cases} \tag{4.1}$$

where the controls u_1, u_2 and u_3 are the target horizontal linear velocity, altitude and yaw angular velocity respectively. The available measurements are the cartesian target coordinate z_1, z_2, z_3, thus, according to (4.1), u_1, u_2, u_3 are clearly observable (we used the local model $\dot{u}_i = 0$, $i = 1, 2, 3$). Note that system (4.1) reduces to the Dubins system when the target moves in a horizontal plane.

4.3 Numerical results

We now present numerical simulations illustrating the tracking algorithm presented in the previous section.

In each case we consider a UAV flying at constant unitary speed and modeled by System (2.1) or System (2.5) depending on the type of UAV we consider (HALE or MALE). We numerically integrate the system during 500 units of time.

For each of the three methods we show simulations for both cases where the target path is known or not. If this information is unknown we use an extended Kalman filter to predict the future target position. Note that the target speed is not assumed to be constant.

On each figure, the dashed circle represents the trajectory to be followed. The results are drawn in the inertial frame (on the left) and in an orthonormal moving frame attached to the target (on the right) in order to observe the positioning error.

Figures 19 and 20 illustrate the time-optimal tracking method for the same UAV starting from the same initial position. The target that we want to track starts at $(z_1, z_2) = (0, 0)$; its behavior is known on Figure 19 and unknown on Figure 20.

The second couple of figures, Figures 21 and 22, illustrate the Lyapunov tracking method for the same UAV starting from the same initial position. The target that we want to track starts at $(\hat{x}_0, \hat{y}_0) = (0, 0)$; its behavior is known on Figure 21 and unknown on Figure 22.

Figure 23 and Figures 24, illustrate the 3D-Lyapunov tracking method for the same MALE UAV starts horizontally from the point $(10, -20, 50)$ with a yaw direction of 0 radian and that has the curvature constraints $u_{1\,\max} = u_{2\,\max} = 0.1$, $u_{3\,\max} = 0.5$, $a_3 = 0.1$. The values of the parameters ε and σ (see Section 2.2) are 1.2 and 1 respectively. The target that we want to track starts at $(0, 0, 0)$ and is supposed to move in an horizontal plane; its behavior is known on Figure 23 and unknown on Figure 24. In each simulation, $\mathcal{C}_t$ lies in the horizontal plane located at an altitude of 10 units over the target .

Finally, Figure 25 shows a tracking trajectory obtained for a MALE UAV which follows a target which is not moving in a plane. Here the drone must be positioned at 10 units above the target .

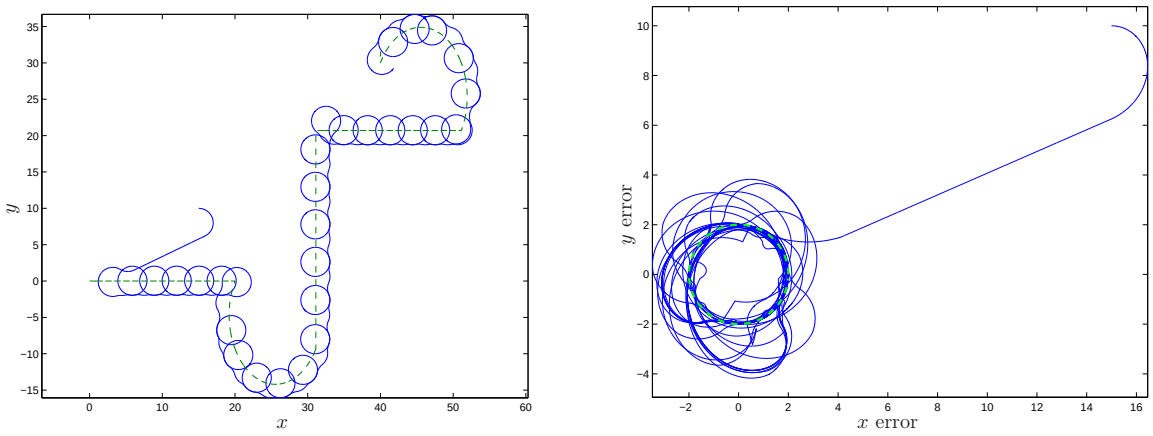

(a) (b)

Figure 19: Time-optimal based tracking method in 2D. UAV's trajectory is continuous, target 's trajectory is dashed and the $\mathcal{C}_t$ is dashed. The behavior of the target is known. $(x_0, y_0, \theta_0) = (15, 10, 0)$, $(z_1, z_2) = (0, 0)$, and $u_{\max} = -a = 0.5$. (a) Trajectories drawn in the (x, y)-coordinates plane. (b) Trajectories drawn in a (orthonormal) frame attached to the center of $\mathcal{C}_t$.

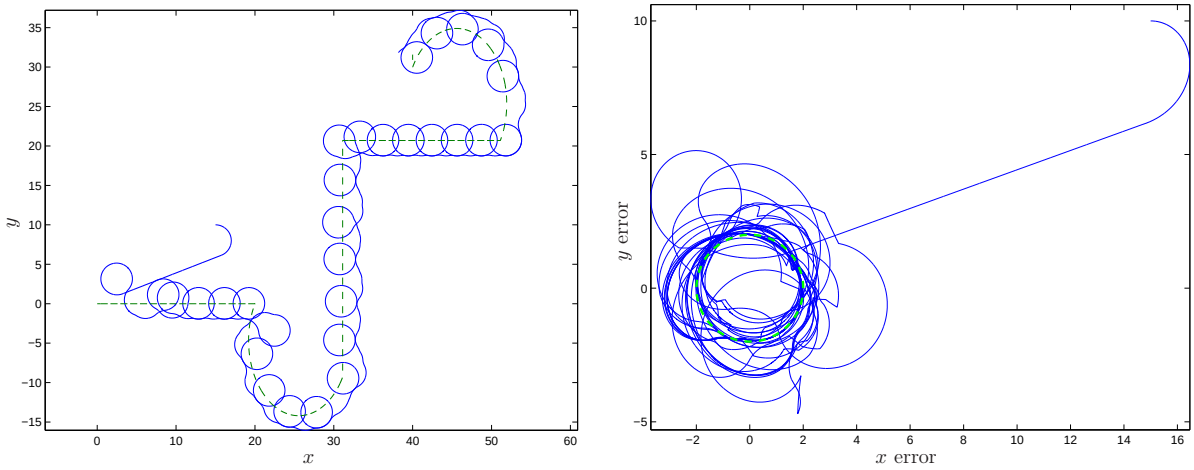

Figure 20: Time-optimal based tracking method in 2D. The only difference with Figure 19 is that, on this figure, the behavior of the target is unknown.

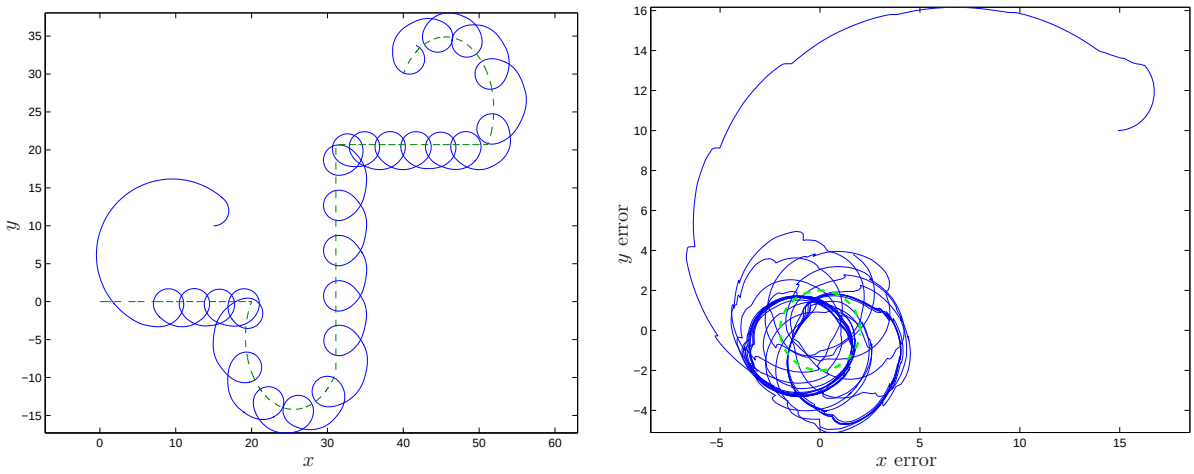

(a) (b)

Figure 21: Lyapunov-LaSalle-based tracking method in 2D. UAV's trajectory is continuous, target 's trajectory is dashed and $\mathcal{C}_t$ is dashed. The behavior of the target is known. $(x_0, y_0, \theta_0) = (15, 10, 0)$, $(z_1, z_2) = (0, 0)$, and $u_{\max} = 0.5$, $a = 0.1$. (a) Trajectories drawn in the (x, y)-coordinates plane. (b) Trajectories drawn in a (orthonormal) frame attached to the center $\mathcal{C}_t$.

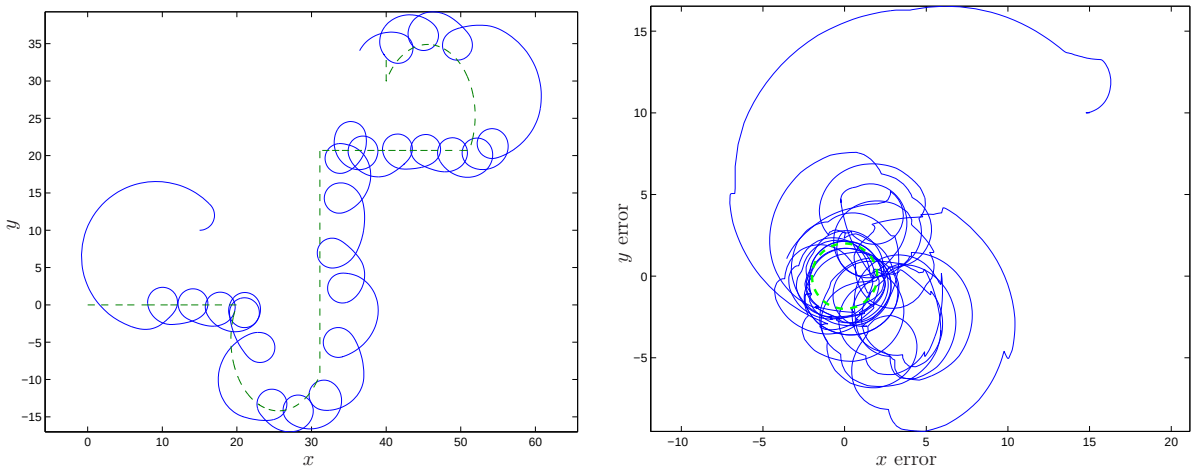

Figure 22: Lyapunov based tracking method in 2D. The only difference with Figure 21 is that, on this figure, the behavior of the target is unknown.

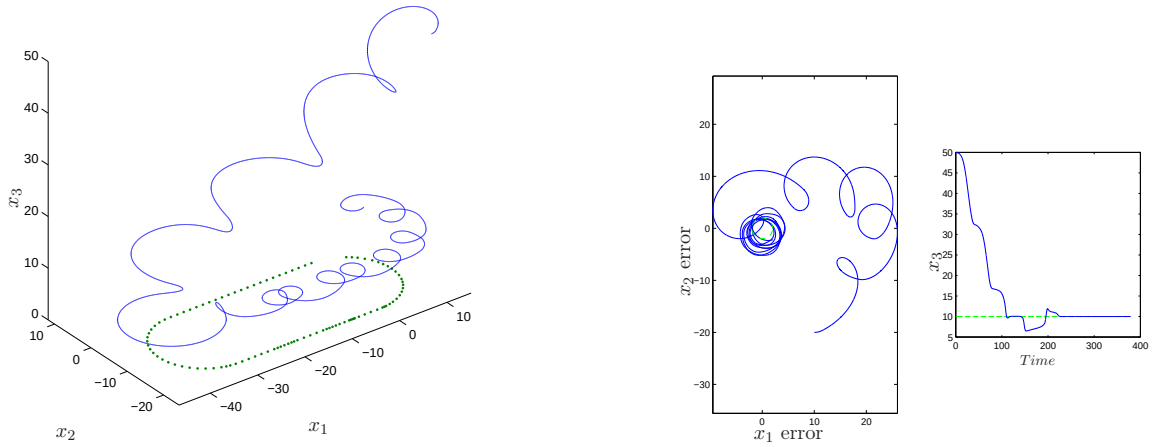

Figure 23: Lyapunov-LaSalle-based tracking method in 3D. The behavior of the target is known.

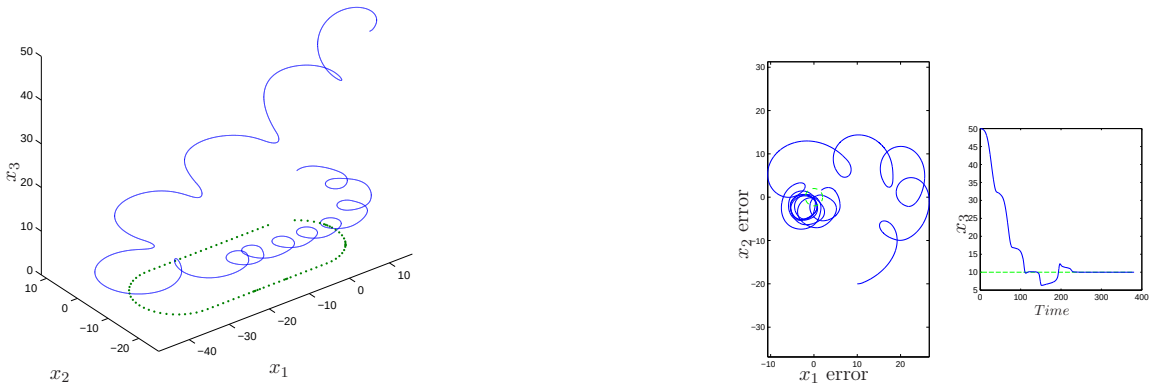

Figure 24: Lyapunov-LaSalle-based tracking method in 3D. The behavior of the target is unknown.

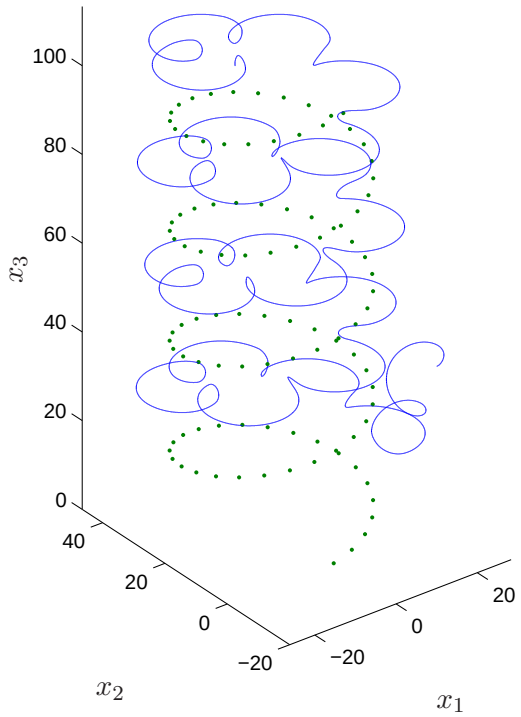

Figure 25: Lyapunov-LaSalle-based tracking method in 3D. The behavior of the target is unknown.

References

[1] A. A. Agrachev and Y. L. Sachkov. *Control theory from the geometric viewpoint*, volume 87 of *Encyclopaedia of Mathematical Sciences*. Springer-Verlag, Berlin, 2004. Control Theory and Optimization, II.

[2] A. A. Agrachev and M. Sigalotti. On the local structure of optimal trajectories in $\mathbf{R}^3$. *SIAM J. Control Optim.*, 42(2):513–531 (electronic), 2003.

[3] A. Ajami, T. Maillot, N. Boizot, J.-F. Balmat, and J.-P. Gauthier. Simulation of a uav ground control station. In *Proceedings of the 9th International Conference of Modeling and Simulation, MOSIM'12*, 2012, *To appear*. Bordeaux, France, 6-8 June, 2012.

[4] K. Ariyur and K. Fregene. Autonomous tracking of a ground vehicle by a uav. In *American Control Conference, 2008*, pages 669 –671, june 2008.

[5] L. Bertuccelli, A. Wu, and J. How. Robust adaptive markov decision processes: Planning with model uncertainty. *Control Systems, IEEE*, 32(5):96–109, 2012.

[6] G. Besancon. *Nonlinear Observers and Applications*. Lecture notes in control and information sciences. Springer London, Limited, 2007.

[7] A. Bhatia, M. Graziano, S. Karaman, R. Naldi, and E. Frazzoli. Dubins trajectory tracking using commercial off-the-shelf autopilots. In *AIAA Guidance, Navigation, and Control Conference*, Honolulu, Hawaii, August 2008.

[8] N. Boizot and J.-P. Gauthier. Motion planning for kinematic systems, 2012.

[9] B. Bonnard, V. Jurdjevic, I. Kupka, and G. Sallet. Transitivity of families of invariant vector fields on the semidirect products of Lie groups. *Trans. Amer. Math. Soc.*, 271(2):525–535, 1982.

[10] U. Boscain and Y. Chitour. Time-optimal synthesis for left-invariant control systems on SO(3). *SIAM J. Control Optim.*, 44(1):111–139 (electronic), 2005.

[11] U. Boscain and B. Piccoli. Extremal synthesis for generic planar systems. *J. Dynam. Control Systems*, 7(2):209–258, 2001.

[12] U. Boscain and B. Piccoli. *Optimal syntheses for control systems on 2-D manifolds*, volume 43 of *Mathématiques & Applications (Berlin) [Mathematics & Applications]*. Springer-Verlag, Berlin, 2004.

[13] A. Bressan and B. Piccoli. A generic classification of time-optimal planar stabilizing feedbacks. *SIAM J. Control Optim.*, 36(1):12–32 (electronic), 1998.

[14] F. Bullo and A. D. Lewis. *Geometric control of mechanical systems*, volume 49 of *Texts in Applied Mathematics*. Springer-Verlag, New York, 2005. Modeling, analysis, and design for simple mechanical control systems.

[15] D. Campolo, L. Schenato, E. Guglielmelli, and S. Sastry. A lyapunov-based approach for the control of biomimetic robotic systems with periodic forcing inputs. In *Proceedings of 16th IFAC World Congress on Automatic Control (IFAC05)*, 2005.

[16] H. Chen, K. Chang, and C. S. Agate. Tracking with uav using tangent-plus-lyapunov vector field guidance. In *Information Fusion, 2009. FUSION '09. 12th International Conference on*, pages 363 –372, july 2009.

[17] H. Chitsaz and S. LaValle. Time-optimal paths for a dubins airplane. In *Decision and Control, 2007 46th IEEE Conference on*, pages 2379 –2384, dec. 2007.

[18] V. Cichella, I. Kaminer, V. Dobrokhodov, E. Xargay, N. Hovakimyan, and A. Pascoal. Geometric 3d path-following control for a fixed-wing uav on so(3). In *AIAA Guidance, Navigation, and Control Conference*. American Institute of Aeronautics and Astronautics, 2013/05/02 2011.

[19] D. V. Dimarogonas, S. G. Loizou, K. J. Kyriakopoulos, and M. M. Zavlanos. A feedback stabilization and collision avoidance scheme for multiple independent non-point agents. *Automatica*, 42(2):229 – 243, 2006.

[20] X. Ding, A. Rahmani, and M. Egerstedt. Multi-uav convoy protection: an optimal approach to path planning and coordination. *Robotics, IEEE Transactions on*, 26(2):256–268, 2010.

[21] E. Frew, D. Lawrence, C. Dixon, J. Elston, and W. Pisano. Lyapunov guidance vector fields for unmanned aircraft applications. In *American Control Conference, 2007. ACC '07*, pages 371 –376, july 2007.

[22] E. Frew, T. McGee, Z. Kim, X. Xiao, S. Jackson, M. Morimoto, S. Rathinam, J. Padial, and R. Sengupta. Vision-based road-following using a small autonomous aircraft. In *Aerospace Conference, 2004. Proceedings. 2004 IEEE*, volume 5, pages 3006 – 3015 Vol.5, march 2004.

[23] E. W. Frew, D. A. Lawrence, and S. Morris. Coordinated standoff tracking of moving targets using lyapunov guidance vector fields. *Journal of Guidance, Control, and Dynamics*, 31(2):290–306, 2013/02/21 2008.

[24] J.-P. Gauthier and I. Kupka. *Deterministic observation theory and applications*. Cambridge University Press, Cambridge, 2001.

[25] J.-P. Gauthier and V. Zakalyukin. On the one-step-bracket-generating motion planning problem. *J. Dyn. Control Syst.*, 11(2):215–235, 2005.

[26] C. Goerzen, Z. Kong, and B. Mettler. A survey of motion planning algorithms from the perspective of autonomous uav guidance. *Journal of Intelligent and Robotic Systems*, 57(1-4):65–100, 2010.

[27] M.-D. Hua, T. Hamel, P. Morin, and C. Samson. A control approach for thrust-propelled underactuated vehicles and its application to vtol drones. *Automatic Control, IEEE Transactions on*, 54(8):1837 –1853, aug. 2009.

[28] M.-D. Hua, T. Hamel, P. Morin, and C. Samson. A control approach for thrust-propelled underactuated vehicles and its application to VTOL drones. *IEEE Trans. Automat. Control*, 54(8):1837–1853, 2009.

[29] K. L. Kokkeby, R. P. Lutter, M. L. Munoz, F. W. Cathey, J. D. Hilliard, and T. L. Olson. System and methods for autonomous tracking and surveillance, 06 2009.

[30] J. P. LaSalle. Stability theory for ordinary differential equations. *J. Differential Equations*, 4:57–65, 1968.

[31] J.-P. Laumond, editor. *Robot motion planning and control*, volume 229 of *Lecture Notes in Control and Information Sciences*. Springer-Verlag London Ltd., London, 1998. Available online at http://www.laas.fr/∼jpl/book.html.

[32] D. Lawrence, E. Frew, and W. Pisano. Lyapunov vector fields for autonomous uav flight control. In *AIAA Guidance, Navigation and Control Conference and Exhibit*. American Institute of Aeronautics and Astronautics, 2013/02/21 2007.

[33] J. Lee, R. Huang, A. Vaughn, X. Xiao, J. K. Hedrick, M. Zennaro, and R. Sengupta. Strategies of path-planning for a uav to track a ground vehicle. *AINS Conference*, 2003, 2003.

[34] S. Park, J. Deyst, and J. P. How. A new nonlinear guidance logic for trajectory tracking. In *AIAA Guidance, Navigation, and Control Conference and Exhibit*. American Institute of Aeronautics and Astronautics, 2004.

[35] B. Piccoli. Classification of generic singularities for the planar time-optimal synthesis. *SIAM J. Control Optim.*, 34(6):1914–1946, 1996.

[36] B. Piccoli and H. J. Sussmann. Regular synthesis and sufficiency conditions for optimality. *SIAM J. Control Optim.*, 39(2):359–410 (electronic), 2000.

[37] C. G. Prévost, A. Desbiens, and D. Gagnon, Ericand Hodouin. Uav optimal cooperative target tracking and collision avoidance of moving objects. In Chung, M. Jin, Misra, and Pradeep, editors, *The International Federation of Automatic Control, Vol. 17*, pages 5724–5729, 2008.

[38] F. Rafi, S. Khan, K. Shafiq, and M. Shah. Autonomous target following by unmanned aerial vehicles. *Unmanned Systems Technology VIII*, 6230(1):623010, 2006.

[39] Y. Sachkov. Control theory on lie groups. *Journal of Mathematical Sciences*, 156:381–439, 2009.

[40] H. Schättler. On the local structure of time-optimal bang-bang trajectories in $\mathbf{R}^3$. *SIAM J. Control Optim.*, 26(1):186–204, 1988.

[41] K. D. Sebesta and N. Boizot. Real-time adaptive high-gain ekf, applied to a quadcopter inertial navigation system. *IEEE Trans. on Indus. Elec.*, To appear.

[42] P. Souères, A. Balluchi, and A. Bicchi. Optimal feedback control for route tracking with a bounded-curvature vehicle. *Internat. J. Control*, 74(10):1009–1019, 2001.

[43] P. Souères and J.-P. Laumond. Shortest paths synthesis for a car-like robot. *IEEE Trans. Automat. Control*, 41(5):672–688, 1996.

[44] H. J. Sussmann. Regular synthesis for time-optimal control of single-input real analytic systems in the plane. *SIAM J. Control Optim.*, 25(5):1145–1162, 1987.

[45] P. Theodorakopoulos and S. Lacroix. A strategy for tracking a ground target with a uav. In *Intelligent Robots and Systems, 2008. IROS 2008. IEEE/RSJ International Conference on*, pages 1254 –1259, sept. 2008.

[46] G. Walsh, R. Montgomery, and S. Sastry. Optimal path planning on matrix lie groups. In *Decision and Control, 1994., Proceedings of the 33rd IEEE Conference on*, volume 2, pages 1258 –1263 vol.2, dec 1994.

[47] E. Xargay, V. Dobrokhodov, I. Kaminer, A. Pascoal, N. Hovakimyan, and C. Cao. Time-critical cooperative control of multiple autonomous vehicles: Robust distributed strategies for path-following control and time-coordination over dynamic communications networks. *Control Systems, IEEE*, 32(5):49–73, 2012.

[48] S. Zhu, D. Wang, and C. Low. Ground target tracking using uav with input constraints. *Journal of Intelligent & Robotic Systems*, 69:417–429, 2013.